

Compressing Neural Networks: Towards Determining the Optimal Layer-wise Decomposition

Lucas Liebenwein*
MIT CSAIL
lucasl@mit.edu

Alaa Maalouf*
University of Haifa
alaamalouf12@gmail.com

Oren Gal
University of Haifa
orengal@alumni.technion.ac.il

Dan Feldman
University of Haifa
dannyf.post@gmail.com

Daniela Rus
MIT CSAIL
rus@mit.edu

Abstract

We present a novel global compression framework for deep neural networks that automatically analyzes each layer to identify the optimal per-layer compression ratio, while simultaneously achieving the desired overall compression. Our algorithm hinges on the idea of compressing each convolutional (or fully-connected) layer by “slicing” its channels into multiple groups and decomposing each group via low-rank decomposition. At the core of our algorithm is the derivation of layer-wise error bounds from the Eckart–Young–Mirsky theorem. We then leverage these bounds to frame the compression problem as an optimization problem where we wish to minimize the maximum compression error across layers and propose an efficient algorithm towards a solution. Our experiments indicate that our method outperforms existing low-rank compression approaches across a wide range of networks and data sets. We believe that our results open up new avenues for future research into the global performance-size trade-offs of modern neural networks.

1 Introduction

Neural network compression entails taking an existing model and reducing its computational and memory footprint in order to enable the deployment of large-scale networks in resource-constrained environments. Beyond inference time efficiency, compression can yield novel insights into the design (Liu et al., 2019b), training (Liebenwein et al., 2021a,b), and theoretical properties (Arora et al., 2018) of neural networks.

Among existing compression techniques – which include quantization (Wu et al., 2016), distillation (Hinton et al., 2015), and pruning (Han et al., 2015) – *low-rank compression* aims at decomposing a layer’s weight tensor into a tuple of smaller low-rank tensors. Such compression techniques may build upon the rich literature on low-rank decomposition and its numerous applications outside deep learning such as dimensionality reduction (Laparra et al., 2015) or spectral clustering (Peng et al., 2015). Moreover, low-rank

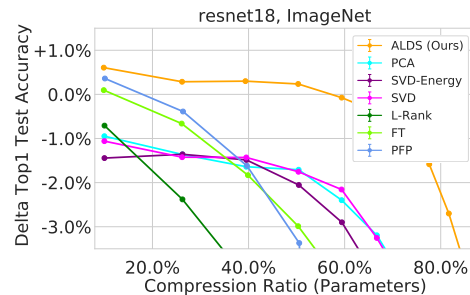


Figure 1: **ALDS**, *Automatic Layer-wise Decomposition Selector*, can compress up to 60% of parameters on a ResNet18 (ImageNet), 3x more compared to baselines. Detailed results are described in Section 3.

*denotes authors with equal contributions. Code: <https://github.com/lucaslie/torchprune>

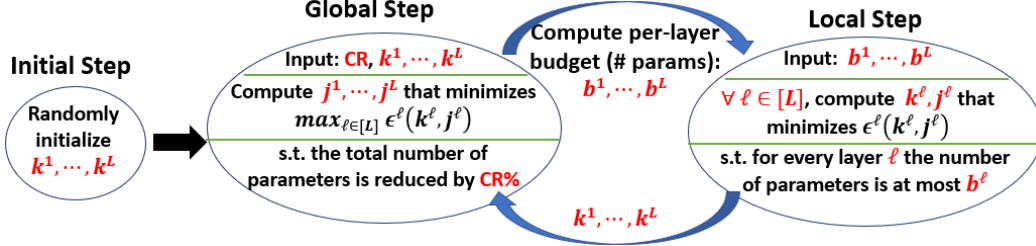


Figure 2: **ALDS Overview**. The framework consists of a global and local step, see Section 2.

compression can be readily implemented in any machine learning framework by replacing the existing layer with a set of smaller layers without the need for, e.g., sparse linear algebra support.

Within deep learning, we encounter two related, yet distinct challenges when applying low-rank compression. On the one hand, each layer should be efficiently decomposed (the “local step”) and, on the other hand, we need to balance the amount of compression in each layer in order to achieve a desired overall compression ratio with minimal loss in the predictive power of the network (the “global step”). While the “local step“, i.e., designing the most efficient layer-wise decomposition method, has traditionally received lots of attention (Denton et al., 2014; Garipov et al., 2016; Jaderberg et al., 2014; Kim et al., 2015b; Lebedev et al., 2015; Novikov et al., 2015), the “global step” has only recently been the focus of attention in research, e.g., see the recent works of Alvarez and Salzmann (2017); Idelbayev and Carreira-Perpinán (2020); Xu et al. (2020).

In this paper, we set out to design a framework that simultaneously accounts for both the local and global step. Our proposed solution, termed *Automatic Layer-wise Decomposition Selector* (ALDS), addresses this challenge by iteratively optimizing for each layer’s decomposition method (local step) and the low-rank compression itself while accounting for the maximum error incurred across layers (global step). In Figure 1, we show how ALDS outperforms existing approaches on the common ResNet18 (ImageNet) benchmark (60% compression compared to $\sim 20\%$ for baselines).

Efficient layer-wise decomposition. Our framework relies on a straightforward SVD-based decomposition of each layer. Inspired by Denton et al. (2014); Idelbayev and Carreira-Perpinán (2020); Jaderberg et al. (2014) and others, we decompose each layer by first folding the weight tensor into a matrix before applying SVD and encoding the resulting pair of matrices as two separate layers.

Enhanced decomposition via multiple subsets. A natural generalization of low-rank decomposition methods entails splitting the matrix into multiple subsets (subspaces) before compressing each subset individually. In the context of deep learning, this was investigated before for individual layers (Denton et al., 2014), including embedding layers (Chen et al., 2018; Maalouf et al., 2021). We take this idea further and incorporate it into our layer-wise decomposition method as additional hyperparameter in terms of the number of subsets. Thus, our local step, i.e., the layer-wise decomposition, constitutes of choosing the number of subsets (k^ℓ) for each layer and the rank (j^ℓ).

Towards a global solution for low-rank compression. We can describe the optimal solution for low-rank compression as the set of hyperparameters (number of subspaces k^ℓ and rank j^ℓ for each layer in our case) that minimizes the drop in accuracy of the compressed network. While finding the globally optimal solution is NP-complete, we propose ALDS as an efficiently solvable alternative that enables us to search for a locally optimal solution in terms of the maximum relative error incurred across layers. To this end, we derive spectral norm bounds based on the Eckhart-Young-Mirsky Theorem for our layer-wise decomposition method to describe the trade-off between the layer compression and the incurred error. Leveraging our bounds we can then efficiently optimize over the set of possible per-layer decompositions. An overview of ALDS is shown in Figure 2.

2 Method

In this section, we introduce our compression framework consisting of a layer-wise decomposition method (Section 2.1), a global selection mechanism to simultaneously compress all layers of a network (Section 2.2), and an optimization procedure (ALDS) to solve the selection problem (Section 2.3).

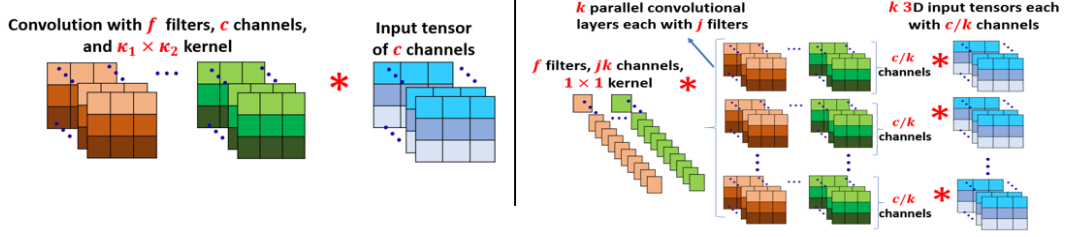


Figure 3: **Left: 2D convolution. right: decomposition used for ALDS.** For a $f \times c \times \kappa_1 \times \kappa_2$ convolution with f filters, c channels, and $\kappa_1 \times \kappa_2$ kernel, our per-layer decomposition consists: (1) k parallel $j \times c/k \times \kappa_1 \times \kappa_2$ convolutions; (2) a single $f \times kj \times 1 \times 1$ convolution applied on the first layer’s (stacked) output.

2.1 Local Layer Compression

We detail our low-rank compression scheme for convolutional layers below and note that it readily applies to fully-connected layers as well as a special case of convolutions with a 1×1 kernel.

Compressing convolutions via SVD. Given a convolutional layer of f filters, c channels, and a $\kappa_1 \times \kappa_2$ kernel we denote the corresponding weight tensor by $\mathcal{W} \in \mathbb{R}^{f \times c \times \kappa_1 \times \kappa_2}$. Following Denton et al. (2014); Idelbayev and Carreira-Perpinán (2020); Wen et al. (2017) and others, we can then interpret the layer as a linear layer of shape $f \times c\kappa_1\kappa_2$ and the corresponding rank j -approximation as two subsequent linear layers of shape $f \times j$ and $j \times c\kappa_1\kappa_2$. Mapped back to convolutions, this corresponds to a $j \times c \times \kappa_1 \times \kappa_2$ convolution followed by a $f \times j \times 1 \times 1$ convolution.

Multiple subspaces. Following the intuition outlined in Section 1 we propose to cluster the columns of the layer’s weight matrix into $k \geq 2$ separate subspaces before applying SVD to each subset. To this end, we may consider any clustering method, such as k-means or projective clustering (Chen et al., 2018; Maalouf et al., 2021). However, such methods require expensive approximation algorithms which would limit our ability to incorporate them into an optimization-based compression framework as outlined in Section 2.2. In addition, arbitrary clustering may require re-shuffling the input tensors which could lead to significant slow-downs during inference. We instead opted for a simple clustering method, namely *channel slicing*, where we simply divide the c input channels of the layer into k subsets each containing at most $\lceil c/k \rceil$ consecutive input channels. Unlike other methods, channel slicing is efficiently implementable, e.g., as grouped convolutions in PyTorch (Paszke et al., 2017) and ensures practical speed-ups subsequent to compressing the network.

Overview of per-layer decomposition. In summary, for given integers $j, k \geq 1$ and a 4D tensor $\mathcal{W} \in \mathbb{R}^{f \times c \times \kappa_1 \times \kappa_2}$ representing a convolution the per-layer compression method proceeds as follows:

1. **PARTITION** the channels of the convolutional layer into k subsets, where each subset has at most $\lceil c/k \rceil$ consecutive channels, resulting in k convolutional tensors $\{\mathcal{W}_i\}_{i=1}^k$ where $\mathcal{W}_i \in \mathbb{R}^{f \times c_i \times \kappa_1 \times \kappa_2}$, and $\sum_{i=1}^k c_i = c$.
2. **DECOMPOSE** each tensor \mathcal{W}_i , $i \in [k]$, by building the corresponding weight matrix $W_i \in \mathbb{R}^{f \times c_i \kappa_1 \kappa_2}$, c.f. Figure 3, computing its j -rank approximation, and factoring it into a pair of smaller matrices U_i of f rows and j columns and V_i of j rows and $c_i \kappa_1 \kappa_2$ columns.
3. **REPLACE** the original layer in the network by 2 layers. The first consists of k parallel convolutions, where the i^{th} parallel layer, $i \in [k]$, is described by the tensor $\mathcal{V}_i \in \mathbb{R}^{j \times c_i \times \kappa_1 \times \kappa_2}$ which can be constructed from the matrix V_i (j filters, c_i channels, $\kappa_1 \times \kappa_2$ kernel). The second layer is constructed by reshaping each matrix U_i , $i \in [k]$, to obtain the tensor $\mathcal{U}_i \in \mathbb{R}^{f \times j \times 1 \times 1}$, and then channel stacking all k tensors $\mathcal{U}_1, \dots, \mathcal{U}_k$ to get a single tensor of shape $f \times kj \times 1 \times 1$.

The decomposed layer is depicted in Figure 3. The resulting layer pair has $jck\kappa_1\kappa_2$ and jfk parameters, respectively, which implies a parameter reduction from $fck\kappa_1\kappa_2$ to $j(fk + ck\kappa_1\kappa_2)$.

2.2 Global Network Compression

In the previous section, we introduced our layer compression scheme. We note that in practice we usually want to compress an entire network consisting of L layers up to a pre-specified relative reduction in parameters (“compression ratio” or CR). However, it is generally unclear how much

each layer $\ell \in [L]$ should be compressed in order to achieve the desired **CR** while incurring a minimal increase in loss. Unfortunately, this optimization problem is NP-complete as we would have to check every combination of layer compression resulting in the desired **CR** in order to optimally compress each layer. On the other hand, simple heuristics, e.g., constant per-layer compression ratios, may lead to sub-optimal results, see Section 3. To this end, we propose an efficiently solvable global compression framework based on minimizing the maximum relative error incurred across layers. We describe each component of our optimization procedure in greater detail below.

The layer-wise relative error as proxy for the overall loss. Since the true cost (the additional loss incurred after compression) would result in an NP-complete problem, we replace the true cost by a more efficient proxy. Specifically, we consider the maximum relative error $\varepsilon := \max_{\ell \in [L]} \varepsilon^\ell$ across layers, where ε^ℓ denotes the theoretical maximum relative error in the ℓ^{th} layer as described in Theorem 1 below. We choose to minimize this particular cost because: (i) minimizing the maximum relative error ensures that no layer incurs an unreasonably large error that might otherwise get propagated or amplified; (ii) relying on a relative instead of an absolute error notion is preferred as scaling between layers may arbitrarily change, e.g., due to batch normalization, and thus the absolute scale of layer errors may not be indicative of the increase in loss; and (iii) the per-layer relative error has been shown to be intrinsically linked to the theoretical compression error, e.g., see the works of Arora et al. (2018) and Baykal et al. (2019a) thus representing a natural proxy for the cost.

Definition of per-layer relative error. Let $\mathcal{W}^\ell \in \mathbb{R}^{f^\ell \times c^\ell \times \kappa_1^\ell \times \kappa_2^\ell}$ and $W^\ell \in \mathbb{R}^{f^\ell \times c^\ell \times \kappa_1^\ell \times \kappa_2^\ell}$ denote the weight tensor and corresponding folded matrix of layer ℓ , respectively. The per-layer relative error ε^ℓ is hereby defined as the relative difference in the operator norm between the matrix \hat{W}^ℓ (that corresponds to the compressed weight tensor $\hat{\mathcal{W}}^\ell$) and the original weight matrix W^ℓ in layer ℓ , i.e.,

$$\varepsilon^\ell := \|\hat{W}^\ell - W^\ell\| / \|W^\ell\|. \quad (1)$$

Note that while in practice our method decomposes the original layer into a set of separate layers (see Section 2.1), for the purpose of deriving the resulting error we re-compose the compressed layers into the overall matrix operator \hat{W}^ℓ , i.e., $\hat{W}^\ell = [U_1^\ell V_1^\ell \cdots U_k^\ell V_k^\ell]$, where $U_i^\ell V_i^\ell$ is the factorization of the i th cluster (set of columns) in the ℓ th layer, for every $\ell \in [L]$ and $i \in [k]$, see supplementary material for more details. We note that the operator norm $\|\cdot\|$ for a convolutional layer thus signifies the maximum relative error incurred for an individual output patch (“pixel”) across all output channels.

Derivation of relative error bounds. We now derive an error bound that enables us to describe the per-layer relative error in terms of the compression hyperparameters j^ℓ and k^ℓ , i.e., $\varepsilon^\ell = \varepsilon^\ell(k^\ell, j^\ell)$. This will prove useful later on as we have to repeatedly query the relative error in our optimization procedure. The error bound is described in the following.

Theorem 1. *Given a layer matrix W^ℓ and the corresponding low-rank approximation \hat{W}^ℓ , the relative error $\varepsilon^\ell := \|\hat{W}^\ell - W^\ell\| / \|W^\ell\|$ is bounded by*

$$\varepsilon^\ell \leq \sqrt{k}/\alpha_1 \cdot \max_{i \in [k]} \alpha_{i,j+1}, \quad (2)$$

where $\alpha_{i,j+1}$ is the $j+1$ largest singular value of the matrix W_i^ℓ , for every $i \in [k]$, and $\alpha_1 = \|W^\ell\|$ is the largest singular value of W^ℓ .

Proof. First, we recall the matrices $W_1^\ell, \dots, W_k^\ell$ and we denote the SVD factorization for each of them by: $W_i^\ell = \tilde{U}_i^\ell \tilde{\Sigma}_i^\ell \tilde{V}_i^\ell$. Now, observe that for every $i \in [k]$, the matrix \hat{W}_i^ℓ is the j -rank approximation of W_i^ℓ . Hence, the SVD factorization of \hat{W}_i^ℓ can be written as $\hat{W}_i^\ell = \tilde{U}_i^\ell \hat{\Sigma}_i^\ell \tilde{V}_i^{\ell T}$, where $\hat{\Sigma}_i^\ell \in \mathbb{R}^{f^\ell \times d}$ is a diagonal matrix such that its first j -diagonal entries are equal to the first j -entries on the diagonal of $\tilde{\Sigma}_i^\ell$, and the rest are zeros. Hence,

$$\begin{aligned} W^\ell - \hat{W}^\ell &= [W_1^\ell - \hat{W}_1^\ell, \dots, W_k^\ell - \hat{W}_k^\ell] = [\tilde{U}_1^\ell (\tilde{\Sigma}_1^\ell - \hat{\Sigma}_1^\ell) \tilde{V}_1^\ell, \dots, \tilde{U}_k^\ell (\tilde{\Sigma}_k^\ell - \hat{\Sigma}_k^\ell) \tilde{V}_k^\ell] \\ &= [\tilde{U}_1^\ell \cdots \tilde{U}_k^\ell] \text{diag} \left((\tilde{\Sigma}_1^\ell - \hat{\Sigma}_1^\ell) \tilde{V}_1^\ell, \dots, (\tilde{\Sigma}_k^\ell - \hat{\Sigma}_k^\ell) \tilde{V}_k^\ell \right). \end{aligned} \quad (3)$$

By (3) and by the triangle inequality, we have that

$$\|W^\ell - \hat{W}^\ell\| \leq \left\| [\tilde{U}_1^\ell \cdots \tilde{U}_k^\ell] \right\| \left\| \text{diag} \left((\tilde{\Sigma}_1^\ell - \hat{\Sigma}_1^\ell) \tilde{V}_1^\ell, \dots, (\tilde{\Sigma}_k^\ell - \hat{\Sigma}_k^\ell) \tilde{V}_k^\ell \right) \right\|. \quad (4)$$

Now, we observe that

$$\left\| \left[\tilde{U}_1^\ell \cdots \tilde{U}_k^\ell \right] \right\|^2 = \left\| \left[\tilde{U}_1^\ell \cdots \tilde{U}_k^\ell \right] \left[\tilde{U}_1^\ell \cdots \tilde{U}_k^\ell \right]^T \right\| = \|\text{diag}(k, \dots, k)\| = k. \quad (5)$$

Finally, we show that

$$\left\| \text{diag} \left((\tilde{\Sigma}_1^\ell - \hat{\Sigma}_1^\ell) \tilde{V}_1^\ell, \dots, (\tilde{\Sigma}_k^\ell - \hat{\Sigma}_k^\ell) \tilde{V}_k^\ell \right) \right\| = \max_{i \in [k]} \left\| (\tilde{\Sigma}_i^\ell - \hat{\Sigma}_i^\ell) \tilde{V}_i^\ell \right\| \quad (6)$$

$$= \max_{i \in [k]} \left\| (\tilde{\Sigma}_i^\ell - \hat{\Sigma}_i^\ell) \right\| = \max_{i \in [k]} \alpha_{i,j+1}, \quad (7)$$

where the second equality holds since the columns of V are orthogonal and the last equality holds according to the Eckhart-Young-Mirsky Theorem (Theorem 2.4.8 of [Golub and Van Loan \(2013\)](#)). Plugging (7) and (5) into (4) concludes the proof. \square

Resulting network size. Let $\theta = \{\mathcal{W}^\ell\}_{\ell=1}^L$ denote the set of weights for the L layers and note that the number of parameters in layer ℓ is given by $|\mathcal{W}^\ell| = f^\ell c^\ell \kappa_1^\ell \kappa_2^\ell$ and $|\theta| = \sum_{\ell \in [L]} |\mathcal{W}^\ell|$. Moreover, note that $|\hat{\mathcal{W}}^\ell| = j^\ell (k^\ell f^\ell + c^\ell \kappa_1^\ell \kappa_2^\ell)$ if decomposed, $\hat{\theta} = \{\hat{\mathcal{W}}^\ell\}_{\ell=1}^L$, and $|\hat{\theta}| = \sum_{\ell \in [L]} |\hat{\mathcal{W}}^\ell|$. The overall compression ratio is thus given by $1 - |\hat{\theta}|/|\theta|$ where we neglected other parameters for ease of exposition. Observe that the layer budget $|\hat{\mathcal{W}}^\ell|$ is fully determined by k^ℓ, j^ℓ just like the error bound.

Global Network Compression. Putting everything together we obtain the following formulation for the optimal per-layer budget:

$$\begin{aligned} \varepsilon_{opt} = \min_{\{j^\ell, k^\ell\}_{\ell=1}^L} \quad & \max_{\ell \in [L]} \varepsilon^\ell(k^\ell, j^\ell) \\ \text{subject to} \quad & 1 - |\hat{\theta}(k^1, j^1, \dots, k^L, j^L)|/|\theta| \leq \mathbf{CR}, \end{aligned} \quad (8)$$

where \mathbf{CR} denotes the desired overall compression ratio. Thus optimally allocating a per-layer budget entails finding the optimal number of subspaces k^ℓ and ranks j^ℓ for each layer constrained by the desired overall compression ratio \mathbf{CR} .

2.3 Automatic Layer-wise Decomposition Selector (ALDS)

We propose to solve (8) by iteratively optimizing k^1, \dots, k^L and j^1, \dots, j^L until convergence akin of an EM-like algorithm as shown in Algorithm 1 and Figure 2. Specifically, for a given set of weights θ and desired compression ratio \mathbf{CR} we first randomly initialize the number of subspaces k^1, \dots, k^L for each layer (Line 2). Based on given values for each k^ℓ we then solve for the optimal ranks j^1, \dots, j^L such that the overall compression ratio is satisfied (Line 4). Note that the maximum error ε is minimized if all errors are equal. Thus solving for the ranks in Line 4 entails guessing a

Algorithm 1 ALDS($\theta, \mathbf{CR}, n_{\text{seed}}$)

Input: θ : network parameters; \mathbf{CR} : overall compression ratio; n_{seed} : number of random seeds to initialize

Output: k^1, \dots, k^L : number of subspaces for each layer; j^1, \dots, j^L : desired rank per subspace for each layer

```

1: for  $i \in [n_{\text{seed}}]$  do
2:    $k^1, \dots, k^L \leftarrow \text{RANDOMINIT}()$ 
3:   while not converged do
4:      $j^1, \dots, j^L \leftarrow \text{OPTIMALRANKS}(\mathbf{CR}, k^1, \dots, k^L)$   $\triangleright$  Global step: choose such that  $\varepsilon^1 = \dots = \varepsilon^L$ 

5:   for  $\ell \in [L]$  do
6:      $b^\ell \leftarrow j^\ell (k^\ell f^\ell + c^\ell \kappa_1^\ell \kappa_2^\ell)$   $\triangleright$  resulting layer budget
7:      $k^\ell \leftarrow \text{OPTIMALSUBSPACES}(b^\ell)$   $\triangleright$  Local step: minimize error bound for a given layer budget
8:   end for
9:   end while
10:   $\varepsilon_i = \text{RECORDERROR}(k^1, \dots, k^L, j^1, \dots, j^L)$ 
11: end for
12: return  $k^1, \dots, k^L, j^1, \dots, j^L$  from  $i_{\text{best}} = \arg\min_i \varepsilon_i$ 

```

value for ε , computing the resulting network size, and repeating the process until the desired CR is satisfied, e.g. via binary search. Subsequently, we re-assign the number of subspaces k^ℓ for each layer by iterating through the finite set of possible values for k^ℓ (Line 7) and choosing the one that minimizes the relative error for the current layer budget b^ℓ (computed in Line 6). We then iteratively repeat both steps until convergence (Lines 3-8). To improve the quality of the local optimum we initialize the procedure with multiple random seeds (Lines 1-11) and pick the allocation with the lowest error (Line 12). We note that we make repeated calls to our decomposition subroutine (i.e. SVD; Lines 4, 7) highlighting the necessity for it to be efficient and cheap to evaluate.

Extensions. Here, we use SVD with multiple subspaces as per-layer compression method. However, we note that ALDS can be readily extended to any desired *set* of low-rank compression techniques. Specifically, we can replace the local step of Line 7 by a search over different methods, e.g., Tucker decomposition, PCA, or other SVD compression schemes, and return the best method for a given budget. In general, we may combine ALDS with any low-rank compression as long as we can efficiently evaluate the per-layer error of the compression scheme. In the supplementary material, we discuss some preliminary results that highlight the promising performance of such extensions.

3 Experiments

Networks and datasets. We study various standard network architectures and data sets. Particularly, we test our compression framework on ResNet20 (He et al., 2016), DenseNet22 (Huang et al., 2017), WRN16-8 (Zagoruyko and Komodakis, 2016), and VGG16 (Simonyan and Zisserman, 2015) on CIFAR10 (Torralba et al., 2008); ResNet18 (He et al., 2016), and AlexNet (Krizhevsky et al., 2012) on ImageNet (Russakovsky et al., 2015); and on Deeplab-V3 (Chen et al., 2017) with a ResNet50 backbone on Pascal VOC segmentation data (Everingham et al., 2015).

Baselines. We compare ALDS to a diverse set of low-rank compression techniques. Specifically, we have implemented PCA (Zhang et al., 2015b), SVD with energy-based layer allocation (SVD-Energy) following Alvarez and Salzmann (2017); Wen et al. (2017), and simple SVD with constant per-layer compression (Denton et al., 2014). Additionally, we also implemented the recent learned rank selection mechanism (L-Rank) of Idelbayev and Carreira-Perpinán (2020). Finally, we implemented two recent filter pruning methods, i.e., FT of Li et al. (2016) and PFP of Liebenwein et al. (2020), as alternative compression techniques for densely compressed networks. Additional comparisons on ImageNet are provided in Section 3.2.

Retraining. For our experiments, we study one-shot and iterative learning rate rewinding inspired by Renda et al. (2020) for various amounts of retraining. In particular, we consider the following unified compress-retrain pipeline across all methods:

1. TRAIN for e epochs according to the standard training schedule for the respective network.
2. COMPRESS the network according to the chosen method.
3. RETRAIN the network for r epochs using the training hyperparameters from epochs $[e - r, e]$.
4. ITERATIVELY repeat 1.-3. after projecting the decomposed layers back (optional).

Reporting metrics. We report Top-1, Top-5, and IoU test accuracy as applicable for the respective task. For each compressed network we also report the compression ratio, i.e., relative reduction, in terms of parameters and floating point operations denoted by CR-P and CR-F, respectively. Each experiment was repeated 3 times and we report mean and standard deviation.

3.1 One-shot Compression on CIFAR10, ImageNet, and VOC with Baselines

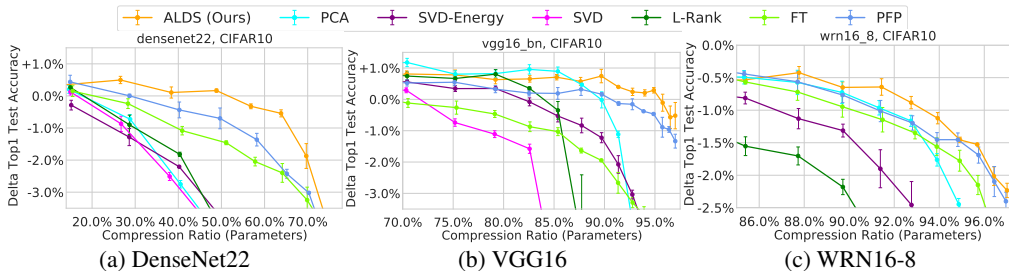


Figure 4: One-shot compress+retrain experiments on CIFAR10 with baseline comparisons.

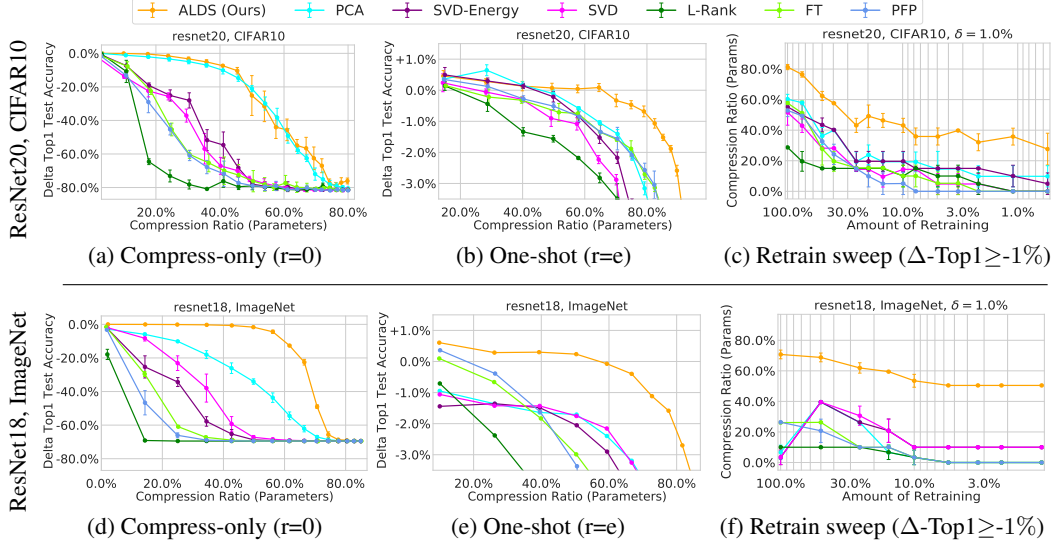


Figure 5: The size-accuracy trade-off for various compression ratios, methods, and networks. Compression was performed after training and networks were re-trained once for the indicated amount (**one-shot**). (a, b, d, e): the difference in test accuracy for fixed amounts of retraining. (c, f): the maximal compression ratio with less-than-1% accuracy drop for variable amounts of retraining.

We train reference networks on CIFAR10, ImageNet, and VOC, and then compress and retrain the networks *once* with $r = e$ for various baseline comparisons and compression ratios. In Figure 4, we provide results for DenseNet22, VGG16, and WRN16-8 on CIFAR10. Notably, our approach is able to outperform existing baselines approaches across a wide range of tested compression ratios.

Specifically, in the region where the networks incur only minimal drop in accuracy ($\Delta\text{-Top1} \geq -1\%$) ALDS is particularly effective.

Moreover, we tested ALDS on ResNet20 (CIFAR10) and ResNet18 (ImageNet) as shown in Figure 5. For these experiments, we performed a grid search over both multiple compression ratios and amounts of retraining. Here, we highlight that ALDS outperforms baseline approaches even with significantly less retraining. On Resnet 18 (ImageNet) ALDS can compress over 50% of the parameters with minimal retraining (1% retraining) and a less-than-1% accuracy drop compared to the best comparison methods (40% compression with 50% retraining). Finally, we tested the same setup on a DeeplabV3 with a ResNet50 backbone trained on Pascal VOC 2012 segmentation data, see Figure 6. We note

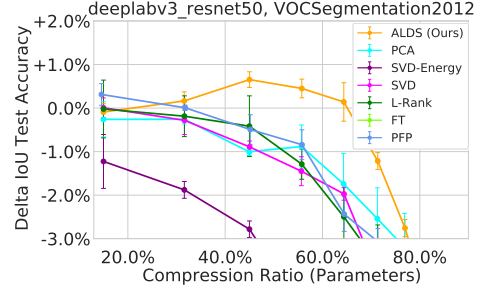


Figure 6: One-shot compress+retrain for DeeplabV3-ResNet50 on VOC.

Table 1: Baseline results for $\Delta\text{-Top1} \geq -0.5\%$ for one-shot. Results coincide with Figures 4, 5, 6.

	Model	Metric	ALDS (Ours)	PCA	SVD-Energy	SVD	L-Rank	FT	PFP
CIFAR10	ResNet20 Top1: 91.39	$\Delta\text{-Top1}$	-0.47	-0.11	-0.21	-0.29	-0.44	-0.32	-0.28
		CR-P, CR-F	74.91, 67.86	49.88, 48.67	49.88, 49.08	39.81, 38.95	28.71, 54.89	39.69, 39.57	40.28, 30.06
	VGG16 Top1: 92.78	$\Delta\text{-Top1}$	-0.11	-0.02	-0.08	+0.29	-0.35	-0.47	-0.47
		CR-P, CR-F	95.77, 86.23	89.72, 85.84	82.57, 81.32	70.35, 70.13	85.38, 75.86	79.13, 78.44	94.87, 84.76
	DenseNet22 Top1: 89.88	$\Delta\text{-Top1}$	-0.32	+0.20	-0.29	+0.13	+0.26	-0.24	-0.44
		CR-P, CR-F	56.84, 61.98	14.67, 34.55	15.16, 19.34	15.00, 15.33	14.98, 35.21	28.33, 29.50	40.24, 43.37
ImageNet	WRN16-8 Top1: 89.88	$\Delta\text{-Top1}$	-0.42	-0.49	-0.41	-0.96	-0.45	-0.32	-0.44
		CR-P, CR-F	87.77, 79.90	85.33, 83.45	64.75, 60.94	40.20, 39.97	49.86, 58.00	82.33, 75.97	85.33, 80.68
	ResNet18 Top1: 69.62, Top5: 89.08	$\Delta\text{-Top1}$, Top5	-0.40, -0.05	-0.95, -0.37	-1.49, -0.64	-1.75, -0.72	-0.71, -0.23	+0.10, +0.42	-0.39, -0.08
		CR-P, CR-F	66.70, 43.51	9.99, 12.78	39.56, 40.99	50.38, 50.37	10.01, 32.64	9.86, 11.17	26.35, 17.96
	DeeplabV3 IoU: 91.39 Top1: 99.34	$\Delta\text{-IoU}$, Top1	+0.14, -0.15	-0.26, -0.02	-1.88, -0.47	-0.28, -0.18	-0.42, -0.09	-4.30, -0.91	-0.49, -0.21
		CR-P, CR-F	64.38, 64.11	55.68, 55.82	31.61, 32.27	31.64, 31.51	44.99, 45.02	15.00, 15.06	45.17, 43.93

that ALDS consistently outperforms other baseline methods in this setting as well (60% CR-P vs. 20% without accuracy drop).

Our one-shot results are again summarized in Table 1 where we report CR-P and CR-F for $\Delta\text{-Top1} \geq -0.5\%$. We note that pruning usually takes on the order of seconds and minutes for CIFAR and ImageNet, respectively, which is usually faster than even a single training epoch.

3.2 ImageNet Benchmarks

Next, we test our framework on two common ImageNet benchmarks, ResNet18 and AlexNet. We follow the compress-retrain pipeline outlined in the beginning of the section and repeat it iteratively to obtain higher compression ratios. Specifically, after retraining and before the next compression step we project the decomposed layers back to the original layer. This way, we avoid recursing on the decomposed layers.

Our results are reported in Table 2 where we compare to a wide variety of available compression benchmarks (results were adapted directly from the respective papers). The middle part and bottom part of the table for each network are organized into low-rank compression and filter pruning approaches, respectively. Note that the reported differences in accuracy ($\Delta\text{-Top1}$ and $\Delta\text{-Top5}$) are relative to our baseline accuracies. On ResNet18 we can reduce the number of FLOPs by 65% with minimal drop in accuracy compared to the best competing method (MUSCO, 58.67%). With a slightly higher drop in accuracy (-1.37%) we can even compress 76% of FLOPs. On AlexNet, our framework finds networks with -0.21% and -0.41% difference in accuracy with over 77% and 81% fewer FLOPs. This constitutes a more-than-10% improvement in terms of FLOPs compared to current state-of-the-art (L-Rank) for similar accuracy drops.

Table 2: AlexNet and ResNet18 Benchmarks on ImageNet. We report Top-1, Top-5 accuracy and percentage reduction of FLOPs (CR-F). Best results with less than 0.5% accuracy drop are bolded.

	Method	$\Delta\text{-Top1}$	$\Delta\text{-Top5}$	CR-F (%)
ResNet18, Top1: 5: 69.64%, 88.98%	ALDS (Ours)	-0.38	+0.04	64.5
	ALDS (Ours)	-1.37	-0.56	76.3
	MUSCO (Gusak et al., 2019)	-0.37	-0.20	58.67
	TRP1 (Xu et al., 2020)	-4.18	-2.5	44.70
	TRP1+Nu (Xu et al., 2020)	-4.25	-2.61	55.15
	TRP2+Nu (Xu et al., 2020)	-4.3	-2.37	68.55
	PCA (Zhang et al., 2015b)	-6.54	-4.54	29.07
	Expand (Jaderberg et al., 2014)	-6.84	-5.26	50.00
	PFP (Liebenwein et al., 2020)	-2.26	-1.07	29.30
	SoftNet (He et al., 2018)	-2.54	-1.2	41.80
	Median (He et al., 2019)	-1.23	-0.5	41.80
	Slimming (Liu et al., 2017)	-1.77	-1.19	28.05
	Low-cost (Dong et al., 2017)	-3.55	-2.2	34.64
	Gating (Hua et al., 2018)	-1.52	-0.93	37.88
	FT (He et al., 2017)	-3.08	-1.75	41.86
	DCP (Zhuang et al., 2018)	-2.19	-1.28	47.08
	FBS (Gao et al., 2018)	-2.44	-1.36	49.49
AlexNet, Top1: 5: 57.30%, 80.20%	ALDS (Ours)	-0.21	-0.36	77.9
	ALDS (Ours)	-0.41	-0.54	81.4
	Tucker (Kim et al., 2015a)	N/A	-1.87	62.40
	Regularize (Tai et al., 2015)	N/A	-0.54	74.35
	Coordinate (Wen et al., 2017)	N/A	-0.34	62.82
	Efficient (Kim et al., 2019)	-0.7	-0.3	62.40
	L-Rank (Idelbayev et al., 2020)	-0.13	-0.13	66.77
	NISP (Yu et al., 2018)	-1.43	N/A	67.94
	OICSR (Li et al., 2019a)	-0.47	N/A	53.70
	Oracle (Ding et al., 2019)	-1.13	-0.67	31.97

3.3 Ablation Study

To investigate the different features of our method we ran compression experiments using multiple variations derived from our method, see Figure 7. For the simplest version of our method we consider a constant per-layer compression ratio and fix the value of k to either 3 or 5 for all layers denoted by ALDS-Simple3 and ALDS-Simple5, respectively. Note that ALDS-Simple with $k = 1$ corresponds to the SVD comparison method. For the version denoted by ALDS-Error3 we fix the number of subspaces per layer ($k = 3$) and only run the global step of ALDS (Line 4 of Algorithm 1) to determine the optimal per-layer compression ratio. The results of our ablation study in Figure 7 indicate that our method clearly benefits from the combination of both the global and local step in terms of the number of subspaces (k) and the rank per subspace (j).

We also compare our subspace clustering (channel slicing) to the clustering technique of Maalouf et al. (2021), which clusters the matrix columns using projective clustering. Specifically, we replace the channel slicing of ALDS-Simple3 with projective clustering (Messi3 in Figure 7). As expected

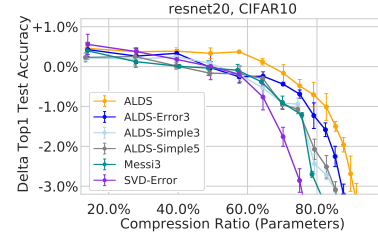


Figure 7: One-shot ablation study of ALDS for Resnet20 (CIFAR10).

Messi improves the performance over ALDS-Simple but only slightly and the difference is essentially negligible. Together with the computational disadvantages of Messi-like clustering methods (unstructured, NP-hard; see Section 2.1) ALDS-based simple channel slicing is therefore the preferred choice in our context.

4 Related Work

Our work builds upon prior work in neural network compression. We discuss related work focusing on pruning, low-rank compression, and global aspects of compression.

Unstructured pruning. Weight pruning (Lin et al., 2020b; Molchanov et al., 2016, 2019; Singh and Alistarh, 2020; Wang et al., 2021; Yu et al., 2018) techniques aim to reduce the number of individual weights, e.g., by removing weights with absolute values below a threshold (Han et al., 2015; Renda et al., 2020), or by using a mini-batch of data points to approximate the influence of each parameter on the loss function (Baykal et al., 2019a,b). However, since these approaches generate sparse instead of smaller models they require some form of sparse linear algebra support for runtime speed-ups.

Structured pruning. Pruning structures such as filters directly shrinks the network (Chen et al., 2020; Li et al., 2019b; Lin et al., 2020a; Liu et al., 2019a; Luo and Wu, 2020; Ye et al., 2018). Filters can be pruned using a score for each filter, e.g., weight-based (He et al., 2018, 2017) or data-informed (Liebenwein et al., 2020; Yu et al., 2018), and removing those with a score below a threshold. It is worth noting that filter pruning is complimentary to low-rank compression.

Low-rank compression (local step). A common approach to low-rank compression entails tensor decomposition including Tucker-decomposition (Kim et al., 2015b), CP-decomposition (Lebedev et al., 2015), Tensor-Train (Garipov et al., 2016; Novikov et al., 2015) and others (Denil et al., 2013; Ioannou et al., 2017; Jaderberg et al., 2014). Other decomposition-like approaches include weight sharing, random projections, and feature hashing (Arora et al., 2018; Chen et al., 2015a,b; Shi et al., 2009; Ullrich et al., 2017; Weinberger et al., 2009). Alternatively, low-rank compression can be performed via matrix decomposition (e.g., SVD) on flattened tensors as done by Denton et al. (2014); Sainath et al. (2013); Tukan et al. (2020); Xue et al. (2013); Yu et al. (2017) among others. Chen et al. (2018); Denton et al. (2014); Maalouf et al. (2021) also explores the use of subspace clustering before applying low-rank compression to each cluster to improve the approximation error. Notably, most prior work relies on some form of expensive approximation algorithm – even to just solve the per-layer low-rank compression, e.g., clustering or tensor decomposition. In this paper, we instead focus on the global compression problem and show that simple compression techniques (SVD with channel slicing) are advantageous in this context as we can use them as efficient subroutines. We note that we can even extend our algorithm to multiple, different types of per-layer decomposition.

Network-aware compression (global step). To determine the rank (or the compression ratio) of each layer, prior work suggests to account for compression during training (Alvarez and Salzmann, 2017; Ioannou et al., 2016, 2015; Wen et al., 2017; Xu et al., 2020), e.g., by training the network with a penalty that encourages the weight matrices to be low-rank. Others suggest to select the ranks using variational Bayesian matrix factorization (Kim et al., 2015b). In their recent paper, Chin et al. (2020) suggest to produce an entire set of compressed networks with different accuracy/speed trade-offs. Our paper was also inspired by a recent line of work towards automatically choosing or learning the rank of each layer (Gusak et al., 2019; Idelbayev and Carreira-Perpinán, 2020; Li and Shi, 2018; Tiwari et al., 2021; Zhang et al., 2015b,c). We take such approaches further and suggest a global compression framework that incorporates multiple decomposition techniques with more than one hyper-parameter per layer (number of subspaces and ranks of each layer). This approach increases the number of local minima in theory and helps improving the performance in practice.

5 Discussion and Conclusion

Practical benefits. By conducting a wide variety of experiments across multiple data sets and networks we have shown the effectiveness and versatility of our compression framework compared to existing methods. The runtime of ALDS is negligible compared to retraining and it can thus be efficiently incorporated into compress-retrain pipelines.

ALDS as modular compression framework. By separately considering the low-rank compression scheme for each layer (local step) and the actual low-rank compression (global step) we have provided a framework that can efficiently search over a set of desired hyperparameters that describe the low-

rank compression. Naturally, our framework can thus be generalized to other compression schemes (such as tensor decomposition) and we hope to explore these aspects in future work.

Error bounds lead to global insights. At the core of our contribution is our error analysis that enables us to link the global and local aspects of layer-wise compression techniques. We leverage our error bounds in practice to compress networks more effectively via an automated rank selection procedure without additional tedious hyperparameter tuning. However, we also have to rely on a proxy definition (maximum relative error) of the compression error to enable a tractable solution that we can implement efficiently. We hope these observations invigorate future research into compression techniques that come with tight error bounds – potentially even considering retraining – which can then naturally be wrapped into a global compression framework.

Acknowledgments

This research was sponsored by the United States Air Force Research Laboratory and the United States Air Force Artificial Intelligence Accelerator and was accomplished under Cooperative Agreement Number FA8750-19-2-1000. The views and conclusions contained in this document are those of the authors and should not be interpreted as representing the official policies, either expressed or implied, of the United States Air Force or the U.S. Government. The U.S. Government is authorized to reproduce and distribute reprints for Government purposes notwithstanding any copyright notation herein. This work was further supported by the Office of Naval Research (ONR) Grant N00014-18-1-2830.

References

- Jose M Alvarez and Mathieu Salzmann. Compression-aware training of deep networks. In *Advances in Neural Information Processing Systems*, pages 856–867, 2017.
- Sanjeev Arora, Rong Ge, Behnam Neyshabur, and Yi Zhang. Stronger generalization bounds for deep nets via a compression approach. In *International Conference on Machine Learning*, pages 254–263, 2018.
- Cenk Baykal, Lucas Liebenwein, Igor Gilitschenski, Dan Feldman, and Daniela Rus. Data-dependent coresets for compressing neural networks with applications to generalization bounds. In *International Conference on Learning Representations*, 2019a. URL <https://openreview.net/forum?id=HJfwJ2A5KX>.
- Cenk Baykal, Lucas Liebenwein, Igor Gilitschenski, Dan Feldman, and Daniela Rus. Sipping neural networks: Sensitivity-informed provable pruning of neural networks. *arXiv preprint arXiv:1910.05422*, 2019b.
- Jianda Chen, Shangyu Chen, and Sinno Jialin Pan. Storage efficient and dynamic flexible runtime channel pruning via deep reinforcement learning. *Advances in Neural Information Processing Systems*, 33, 2020.
- Liang-Chieh Chen, George Papandreou, Florian Schroff, and Hartwig Adam. Rethinking atrous convolution for semantic image segmentation. *arXiv preprint arXiv:1706.05587*, 2017.
- Patrick H. Chen, Si Si, Yang Li, Ciprian Chelba, and Cho-jui Hsieh. GroupReduce: Block-Wise Low-Rank Approximation for Neural Language Model Shrinking. *Advances in Neural Information Processing Systems*, 2018-December:10988–10998, jun 2018. URL <http://arxiv.org/abs/1806.06950>.
- Wenlin Chen, James Wilson, Stephen Tyree, Kilian Weinberger, and Yixin Chen. Compressing neural networks with the hashing trick. In *International conference on machine learning*, pages 2285–2294, 2015a.
- Wenlin Chen, James T. Wilson, Stephen Tyree, Kilian Q. Weinberger, and Yixin Chen. Compressing convolutional neural networks. *CoRR*, abs/1506.04449, 2015b. URL <http://arxiv.org/abs/1506.04449>.

- Ting-Wu Chin, Ruizhou Ding, Cha Zhang, and Diana Marculescu. Towards efficient model compression via learned global ranking. In *Proceedings of the IEEE/CVF Conference on Computer Vision and Pattern Recognition*, pages 1518–1528, 2020.
- Kenneth L Clarkson and David P Woodruff. Input sparsity and hardness for robust subspace approximation. In *2015 IEEE 56th Annual Symposium on Foundations of Computer Science*, pages 310–329. IEEE, 2015.
- Arthur P Dempster, Nan M Laird, and Donald B Rubin. Maximum likelihood from incomplete data via the em algorithm. *Journal of the Royal Statistical Society: Series B (Methodological)*, 39(1): 1–22, 1977.
- Misha Denil, Babak Shakibi, Laurent Dinh, Marc Aurelio Ranzato, and Nando de Freitas. Predicting parameters in deep learning. In *Advances in Neural Information Processing Systems 26*, pages 2148–2156, 2013.
- Emily Denton, Wojciech Zaremba, Joan Bruna, Yann LeCun, and Rob Fergus. Exploiting Linear Structure Within Convolutional Networks for Efficient Evaluation. *Advances in Neural Information Processing Systems*, 2(January):1269–1277, apr 2014. URL <http://arxiv.org/abs/1404.0736>.
- Xiaohan Ding, Guiguang Ding, Yuchen Guo, Jungong Han, and Chenggang Yan. Approximated oracle filter pruning for destructive cnn width optimization. In *International Conference on Machine Learning*, pages 1607–1616. PMLR, 2019.
- Xuanyi Dong, Junshi Huang, Yi Yang, and Shuicheng Yan. More is less: A more complicated network with less inference complexity. In *Proceedings of the IEEE Conference on Computer Vision and Pattern Recognition*, pages 5840–5848, 2017.
- Mark Everingham, SM Ali Eslami, Luc Van Gool, Christopher KI Williams, John Winn, and Andrew Zisserman. The pascal visual object classes challenge: A retrospective. *International journal of computer vision*, 111(1):98–136, 2015.
- Xitong Gao, Yiren Zhao, Łukasz Dudziak, Robert Mullins, and Cheng-zhong Xu. Dynamic channel pruning: Feature boosting and suppression. *arXiv preprint arXiv:1810.05331*, 2018.
- Timur Garipov, Dmitry Podoprikhin, Alexander Novikov, and Dmitry Vetrov. Ultimate tensorization: compressing convolutional and fc layers alike. *arXiv preprint arXiv:1611.03214*, 2016.
- Gene H Golub and Charles F Van Loan. *Matrix computations*, volume 3. JHU press, 2013.
- Priya Goyal, Piotr Dollár, Ross Girshick, Pieter Noordhuis, Lukasz Wesolowski, Aapo Kyrola, Andrew Tulloch, Yangqing Jia, and Kaiming He. Accurate, large minibatch sgd: Training imagenet in 1 hour. *arXiv preprint arXiv:1706.02677*, 2017.
- Julia Gusak, Maksym Kholiavchenko, Evgeny Ponomarev, Larisa Markeeva, Philip Blagoveschensky, Andrzej Cichocki, and Ivan Oseledets. Automated multi-stage compression of neural networks. In *Proceedings of the IEEE/CVF International Conference on Computer Vision Workshops*, pages 0–0, 2019.
- Song Han, Huizi Mao, and William J. Dally. Deep compression: Compressing deep neural network with pruning, trained quantization and Huffman coding. *CoRR*, abs/1510.00149, 2015. URL <http://arxiv.org/abs/1510.00149>.
- Bharath Hariharan, Pablo Arbeláez, Lubomir Bourdev, Subhransu Maji, and Jitendra Malik. Semantic contours from inverse detectors. In *2011 International Conference on Computer Vision*, pages 991–998. IEEE, 2011.
- Kaiming He, Xiangyu Zhang, Shaoqing Ren, and Jian Sun. Deep residual learning for image recognition. In *Proceedings of the IEEE conference on computer vision and pattern recognition*, pages 770–778, 2016.
- Yang He, Guoliang Kang, Xuanyi Dong, Yanwei Fu, and Yi Yang. Soft filter pruning for accelerating deep convolutional neural networks. In *Proceedings of the 27th International Joint Conference on Artificial Intelligence*, pages 2234–2240. AAAI Press, 2018.

- Yang He, Ping Liu, Ziwei Wang, Zhilan Hu, and Yi Yang. Filter pruning via geometric median for deep convolutional neural networks acceleration. In *Proceedings of the IEEE Conference on Computer Vision and Pattern Recognition*, pages 4340–4349, 2019.
- Yihui He, Xiangyu Zhang, and Jian Sun. Channel pruning for accelerating very deep neural networks. In *Proceedings of the IEEE International Conference on Computer Vision*, pages 1389–1397, 2017.
- Geoffrey Hinton, Oriol Vinyals, and Jeff Dean. Distilling the knowledge in a neural network. *arXiv preprint arXiv:1503.02531*, 2015.
- Weizhe Hua, Yuan Zhou, Christopher De Sa, Zhiru Zhang, and G Edward Suh. Channel gating neural networks. *arXiv preprint arXiv:1805.12549*, 2018.
- Gao Huang, Zhuang Liu, Laurens Van Der Maaten, and Kilian Q Weinberger. Densely connected convolutional networks. In *Proceedings of the IEEE conference on computer vision and pattern recognition*, pages 4700–4708, 2017.
- Yerlan Idelbayev and Miguel A Carreira-Perpinán. Low-rank compression of neural nets: Learning the rank of each layer. In *Proceedings of the IEEE/CVF Conference on Computer Vision and Pattern Recognition*, pages 8049–8059, 2020.
- Y Ioannou, D Robertson, J Shotton, R Cipolla, and A Criminisi. Training cnns with low-rank filters for efficient image classification. In *4th International Conference on Learning Representations, ICLR 2016-Conference Track Proceedings*, 2016.
- Yani Ioannou, Duncan Robertson, Jamie Shotton, Roberto Cipolla, and Antonio Criminisi. Training cnns with low-rank filters for efficient image classification. *arXiv preprint arXiv:1511.06744*, 2015.
- Yani Ioannou, Duncan Robertson, Roberto Cipolla, and Antonio Criminisi. Deep roots: Improving cnn efficiency with hierarchical filter groups. In *Proceedings of the IEEE conference on computer vision and pattern recognition*, pages 1231–1240, 2017.
- Max Jaderberg, Andrea Vedaldi, and Andrew Zisserman. Speeding up convolutional neural networks with low rank expansions. In *Proceedings of the British Machine Vision Conference. BMVA Press*, 2014.
- Hyeji Kim, Muhammad Umar Karim Khan, and Chong-Min Kyung. Efficient neural network compression. In *Proceedings of the IEEE/CVF Conference on Computer Vision and Pattern Recognition*, pages 12569–12577, 2019.
- Yong-Deok Kim, Eunhyeok Park, Sungjoo Yoo, Taelim Choi, Lu Yang, and Dongjun Shin. Compression of Deep Convolutional Neural Networks for Fast and Low Power Mobile Applications. *4th International Conference on Learning Representations, ICLR 2016 - Conference Track Proceedings*, nov 2015a. URL <http://arxiv.org/abs/1511.06530>.
- Yong-Deok Kim, Eunhyeok Park, Sungjoo Yoo, Taelim Choi, Lu Yang, and Dongjun Shin. Compression of deep convolutional neural networks for fast and low power mobile applications. *arXiv preprint arXiv:1511.06530*, 2015b.
- Alex Krizhevsky, Ilya Sutskever, and Geoffrey E Hinton. Imagenet classification with deep convolutional neural networks. In F. Pereira, C. J. C. Burges, L. Bottou, and K. Q. Weinberger, editors, *Advances in Neural Information Processing Systems 25*, pages 1097–1105. Curran Associates, Inc., 2012. URL <http://papers.nips.cc/paper/4824-imagenet-classification-with-deep-convolutional-neural-networks.pdf>.
- Valero Laparra, Jesús Malo, and Gustau Camps-Valls. Dimensionality reduction via regression in hyperspectral imagery. *IEEE Journal of Selected Topics in Signal Processing*, 9(6):1026–1036, 2015.
- Vadim Lebedev, Yaroslav Ganin, Maksim Rakhuba, Ivan V. Oseledets, and Victor S. Lempitsky. Speeding-up convolutional neural networks using fine-tuned cp-decomposition. In *ICLR (Poster)*, 2015. URL <http://arxiv.org/abs/1412.6553>.

- Chong Li and CJ Shi. Constrained optimization based low-rank approximation of deep neural networks. In *Proceedings of the European Conference on Computer Vision (ECCV)*, pages 732–747, 2018.
- Hao Li, Asim Kadav, Igor Durdanovic, Hanan Samet, and Hans Peter Graf. Pruning filters for efficient convnets. *arXiv preprint arXiv:1608.08710*, 2016.
- Jiashi Li, Qi Qi, Jingyu Wang, Ce Ge, Yujian Li, Zhangzhang Yue, and Haifeng Sun. Oicsr: Out-in-channel sparsity regularization for compact deep neural networks. In *Proceedings of the IEEE/CVF Conference on Computer Vision and Pattern Recognition*, pages 7046–7055, 2019a.
- Yawei Li, Shuhang Gu, Luc Van Gool, and Radu Timofte. Learning filter basis for convolutional neural network compression. In *Proceedings of the IEEE International Conference on Computer Vision*, pages 5623–5632, 2019b.
- Lucas Liebenwein, Cenk Baykal, Harry Lang, Dan Feldman, and Daniela Rus. Provable filter pruning for efficient neural networks. In *International Conference on Learning Representations*, 2020. URL <https://openreview.net/forum?id=BJxk01SYDH>.
- Lucas Liebenwein, Cenk Baykal, Brandon Carter, David Gifford, and Daniela Rus. Lost in pruning: The effects of pruning neural networks beyond test accuracy. *Proceedings of Machine Learning and Systems*, 3, 2021a.
- Lucas Liebenwein, Ramin Hasani, Alexander Amini, and Daniela Rus. Sparse flows: Pruning continuous-depth models. *arXiv preprint arXiv:2106.12718*, 2021b.
- Mingbao Lin, Rongrong Ji, Yan Wang, Yichen Zhang, Baochang Zhang, Yonghong Tian, and Ling Shao. Hrank: Filter pruning using high-rank feature map. In *Proceedings of the IEEE/CVF Conference on Computer Vision and Pattern Recognition*, pages 1529–1538, 2020a.
- Tao Lin, Sebastian U. Stich, Luis Barba, Daniil Dmitriev, and Martin Jaggi. Dynamic model pruning with feedback. In *International Conference on Learning Representations*, 2020b. URL <https://openreview.net/forum?id=SJem81SFwB>.
- Zechun Liu, Haoyuan Mu, Xiangyu Zhang, Zichao Guo, Xin Yang, Kwang-Ting Cheng, and Jian Sun. Metapruning: Meta learning for automatic neural network channel pruning. In *Proceedings of the IEEE/CVF International Conference on Computer Vision*, pages 3296–3305, 2019a.
- Zhuang Liu, Jianguo Li, Zhiqiang Shen, Gao Huang, Shoumeng Yan, and Changshui Zhang. Learning efficient convolutional networks through network slimming. In *Proceedings of the IEEE International Conference on Computer Vision*, pages 2736–2744, 2017.
- Zhuang Liu, Mingjie Sun, Tinghui Zhou, Gao Huang, and Trevor Darrell. Rethinking the value of network pruning. In *International Conference on Learning Representations*, 2019b. URL <https://openreview.net/forum?id=rJlnB3C5Ym>.
- Jian-Hao Luo and Jianxin Wu. Autopruner: An end-to-end trainable filter pruning method for efficient deep model inference. *Pattern Recognition*, 107:107461, 2020.
- Alaa Maalouf, Harry Lang, Daniela Rus, and Dan Feldman. Deep learning meets projective clustering. In *International Conference on Learning Representations*, 2021. URL <https://openreview.net/forum?id=EQfpYwF3-b>.
- Pavlo Molchanov, Stephen Tyree, Tero Karras, Timo Aila, and Jan Kautz. Pruning convolutional neural networks for resource efficient inference. *arXiv preprint arXiv:1611.06440*, 2016.
- Pavlo Molchanov, Arun Mallya, Stephen Tyree, Iuri Frosio, and Jan Kautz. Importance estimation for neural network pruning. In *Proceedings of the IEEE Conference on Computer Vision and Pattern Recognition*, pages 11264–11272, 2019.
- Alexander Novikov, Dmitry Podoprikin, Anton Osokin, and Dmitry Vetrov. Tensorizing neural networks. In *Proceedings of the 28th International Conference on Neural Information Processing Systems-Volume 1*, pages 442–450, 2015.

- Adam Paszke, Sam Gross, Soumith Chintala, Gregory Chanan, Edward Yang, Zachary DeVito, Zeming Lin, Alban Desmaison, Luca Antiga, and Adam Lerer. Automatic differentiation in pytorch. In *NIPS-W*, 2017.
- Xi Peng, Zhang Yi, and Huajin Tang. Robust subspace clustering via thresholding ridge regression. In *Twenty-Ninth AAAI Conference on Artificial Intelligence*, 2015.
- Alex Renda, Jonathan Frankle, and Michael Carbin. Comparing fine-tuning and rewinding in neural network pruning. In *International Conference on Learning Representations*, 2020. URL <https://openreview.net/forum?id=SigSjONKvB>.
- Olga Russakovsky, Jia Deng, Hao Su, Jonathan Krause, Sanjeev Satheesh, Sean Ma, Zhiheng Huang, Andrej Karpathy, Aditya Khosla, Michael Bernstein, Alexander C. Berg, and Li Fei-Fei. ImageNet Large Scale Visual Recognition Challenge. *International Journal of Computer Vision (IJCV)*, 115(3):211–252, 2015. doi: 10.1007/s11263-015-0816-y.
- Tara N Sainath, Brian Kingsbury, Vikas Sindhwani, Ebru Arisoy, and Bhuvana Ramabhadran. Low-rank matrix factorization for deep neural network training with high-dimensional output targets. In *2013 IEEE international conference on acoustics, speech and signal processing*, pages 6655–6659. IEEE, 2013.
- Qinfeng Shi, James Petterson, Gideon Dror, John Langford, Alex Smola, and SVN Vishwanathan. Hash kernels for structured data. *Journal of Machine Learning Research*, 10(Nov):2615–2637, 2009.
- Karen Simonyan and Andrew Zisserman. Very deep convolutional networks for large-scale image recognition. *arXiv preprint arXiv:1409.1556*, 2014.
- Karen Simonyan and Andrew Zisserman. Very deep convolutional networks for large-scale image recognition. In *International Conference on Learning Representations*, 2015.
- Sidak Pal Singh and Dan Alistarh. Woodfisher: Efficient second-order approximations for model compression. *arXiv preprint arXiv:2004.14340*, 2020.
- Cheng Tai, Tong Xiao, Yi Zhang, Xiaogang Wang, et al. Convolutional neural networks with low-rank regularization. *arXiv preprint arXiv:1511.06067*, 2015.
- Rishabh Tiwari, Udbhav Bamba, Arnav Chavan, and Deepak Gupta. Chipnet: Budget-aware pruning with heaviside continuous approximations. In *International Conference on Learning Representations*, 2021. URL <https://openreview.net/forum?id=xCxXwTzx4L1>.
- Antonio Torralba, Rob Fergus, and William T Freeman. 80 million tiny images: A large data set for nonparametric object and scene recognition. *IEEE transactions on pattern analysis and machine intelligence*, 30(11):1958–1970, 2008.
- Murad Tukan, Alaa Maalouf, Matan Weksler, and Dan Feldman. Compressed deep networks: Goodbye svd, hello robust low-rank approximation. *arXiv preprint arXiv:2009.05647*, 2020.
- Karen Ullrich, Edward Meeds, and Max Welling. Soft weight-sharing for neural network compression. *arXiv preprint arXiv:1702.04008*, 2017.
- Huan Wang, Can Qin, Yulun Zhang, and Yun Fu. Neural pruning via growing regularization. In *International Conference on Learning Representations*, 2021. URL https://openreview.net/forum?id=o966_Is_nPA.
- Kilian Weinberger, Anirban Dasgupta, John Langford, Alex Smola, and Josh Attenberg. Feature hashing for large scale multitask learning. In *Proceedings of the 26th annual international conference on machine learning*, pages 1113–1120, 2009.
- Wei Wen, Cong Xu, Chunpeng Wu, Yandan Wang, Yiran Chen, and Hai Li. Coordinating Filters for Faster Deep Neural Networks. *Proceedings of the IEEE International Conference on Computer Vision*, 2017-Octob:658–666, mar 2017. URL <http://arxiv.org/abs/1703.09746>.

- Jiaxiang Wu, Cong Leng, Yuhang Wang, Qinghao Hu, and Jian Cheng. Quantized Convolutional Neural Networks for Mobile Devices. In *Proceedings of the International Conference on Computer Vision and Pattern Recognition (CVPR)*, 2016.
- Yuhui Xu, Yuxi Li, Shuai Zhang, Wei Wen, Botao Wang, Yingyong Qi, Yiran Chen, Weiyao Lin, and Hongkai Xiong. TRP: Trained Rank Pruning for Efficient Deep Neural Networks. *IJCAI International Joint Conference on Artificial Intelligence*, 2021-Janua:977–983, apr 2020. URL <http://arxiv.org/abs/2004.14566>.
- Jian Xue, Jinyu Li, and Yifan Gong. Restructuring of deep neural network acoustic models with singular value decomposition. In *Interspeech*, pages 2365–2369, 2013.
- Jianbo Ye, Xin Lu, Zhe Lin, and James Z. Wang. Rethinking the smaller-norm-less-informative assumption in channel pruning of convolution layers. In *International Conference on Learning Representations*, 2018. URL <https://openreview.net/forum?id=HJ94fqApW>.
- Ruichi Yu, Ang Li, Chun-Fu Chen, Jui-Hsin Lai, Vlad I Morariu, Xintong Han, Mingfei Gao, Ching-Yung Lin, and Larry S Davis. Nisp: Pruning networks using neuron importance score propagation. In *Proceedings of the IEEE Conference on Computer Vision and Pattern Recognition*, pages 9194–9203, 2018.
- Xiyu Yu, Tongliang Liu, Xinchao Wang, and Dacheng Tao. On compressing deep models by low rank and sparse decomposition. In *Proceedings of the IEEE Conference on Computer Vision and Pattern Recognition*, pages 7370–7379, 2017.
- Sergey Zagoruyko and Nikos Komodakis. Wide residual networks. *arXiv preprint arXiv:1605.07146*, 2016.
- Xiangyu Zhang, Jianhua Zou, Kaiming He, and Jian Sun. Accelerating Very Deep Convolutional Networks for Classification and Detection. *IEEE Transactions on Pattern Analysis and Machine Intelligence*, 38(10):1943–1955, may 2015a. URL <http://arxiv.org/abs/1505.06798>.
- Xiangyu Zhang, Jianhua Zou, Kaiming He, and Jian Sun. Accelerating very deep convolutional networks for classification and detection. *IEEE transactions on pattern analysis and machine intelligence*, 38(10):1943–1955, 2015b.
- Xiangyu Zhang, Jianhua Zou, Xiang Ming, Kaiming He, and Jian Sun. Efficient and accurate approximations of nonlinear convolutional networks. In *Proceedings of the IEEE Conference on Computer Vision and pattern Recognition*, pages 1984–1992, 2015c.
- Zhuangwei Zhuang, Mingkui Tan, Bohan Zhuang, Jing Liu, Yong Guo, Qingyao Wu, Junzhou Huang, and Jinhui Zhu. Discrimination-aware channel pruning for deep neural networks. *arXiv preprint arXiv:1810.11809*, 2018.

Supplementary Material

Contents

1	Introduction	1
2	Method	2
2.1	Local Layer Compression	3
2.2	Global Network Compression	3
2.3	Automatic Layer-wise Decomposition Selector (ALDS)	5
3	Experiments	6
3.1	One-shot Compression on CIFAR10, ImageNet, and VOC with Baselines	6
3.2	ImageNet Benchmarks	8
3.3	Ablation Study	8
4	Related Work	9
5	Discussion and Conclusion	9
A	Further Method Details	17
A.1	Method Preliminaries	17
A.2	Clustering Methods	18
A.3	Compressing via SVD	19
A.4	Efficient Implementation of ALDS (Algorithm 1)	19
A.5	Extensions of ALDS	20
B	Experimental Setup and Hyperparameters	20
B.1	Experimental Setup for CIFAR10	21
B.2	Experimental Setup for ImageNet	21
B.3	Experimental Setup for Pascal VOC	21
B.4	Baseline Methods	22
B.5	Compress-Retrain Pipeline	23
C	Additional Experimental Results	23
C.1	Complete Tables for One-shot Compression Experiments from Section 3.1	23
C.2	Complete ImageNet Benchmark Results from Section 3.2	26
C.3	Ablation Study	26
C.4	Extensions of ALDS	28

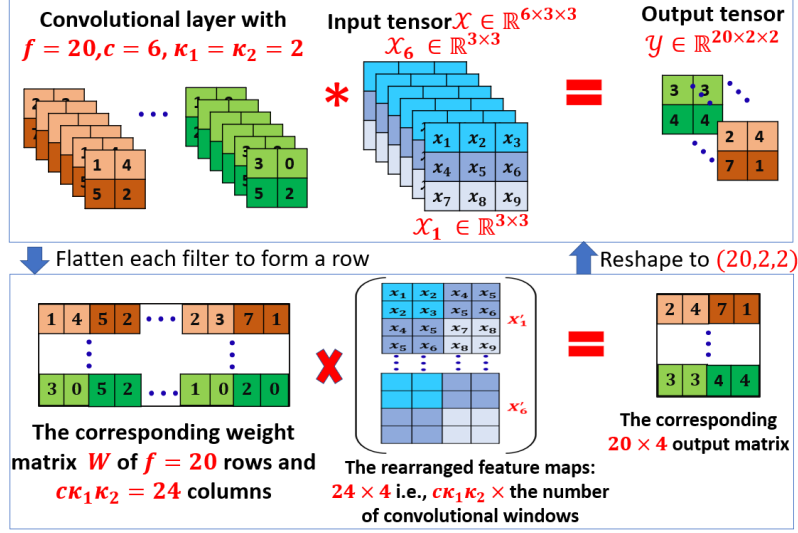


Figure 8: **Convolution to matrix multiplication.** A convolutional layer of $f = 20$ filters, $c = 6$ channels, and 2×2 kernel ($\kappa_1 = \kappa_2 = 2$). The input tensor shape is $6 \times 3 \times 3$. The corresponding weight matrix has $f = 20$ rows (one row per filter) and 24 columns ($c \times \kappa_1 \times \kappa_2$), as for the corresponding feature matrix, it has 24 rows and 4 columns, the 4 here is the number of convolution windows (i.e., number of pixels/entries in each of the output feature maps). After multiplying those matrices, we reshape them to the desired shape to obtain the desired output feature maps.

A Further Method Details

In this section, we provide more details pertaining to our method.

A.1 Method Preliminaries

Our layer-wise compression technique hinges upon the insight that any linear layer may be cast as a matrix multiplication, which enables us to rely on SVD as compression subroutine. Focusing on convolutions we show how such a layer can be recast as matrix multiplication. Similar approaches have been used by [Denton et al. \(2014\)](#); [Idelbayev and Carreira-Perpinán \(2020\)](#); [Wen et al. \(2017\)](#) among others.

Convolution to matrix multiplication. For a given convolutional layer of f filters, c channels, $\kappa_1 \times \kappa_2$ kernel and an input feature map with c features, each of size $m_1 \times m_2$, we denote by $\mathcal{W} \in \mathbb{R}^{f \times c \times \kappa_1 \times \kappa_2}$ and $\mathcal{X} \in \mathbb{R}^{c \times m_1 \times m_2}$ the weight tensor and input tensor, respectively. Moreover, let $W \in \mathbb{R}^{f \times c\kappa_1\kappa_2}$ denote the unfolded matrix operator of the layer constructed from \mathcal{W} by flattening the c kernels of each filter into a row and stacking the rows to form a matrix. Finally, let p denote the total number of sliding blocks and $X \in \mathbb{R}^{c\kappa_1\kappa_2 \times p}$ denote the unfolded input matrix, which is constructed from the input tensor \mathcal{X} as follows: while simulating the convolution by sliding \mathcal{W} along \mathcal{X} we extract the sliding local blocks of \mathcal{X} across all channels by flattening each block into a $c\kappa_1\kappa_2$ -dimensional column vector and concatenating them together to form X . As illustrated in Figure 8 we may now express the convolution $\mathcal{Y} = \mathcal{W} * \mathcal{X}$ as the matrix multiplication $Y = WX$, where $\mathcal{Y} \in \mathbb{R}^{f \times p_1 \times p_2}$ and $Y \in \mathbb{R}^{f \times p}$ correspond to the tensor and matrix representation of the output feature maps, respectively, and p_1, p_2 denote the spatial dimensions of \mathcal{Y} . The equivalence of \mathcal{Y} and Y can be easily established via an appropriate reshaping operation since $p = p_1 p_2$.

Efficient tensor decomposition via SVD. Equipped with the notion of correspondence between convolution and matrix multiplication our goal is to decompose the layer via its matrix operator $W \in \mathbb{R}^{f \times c\kappa_1\kappa_2}$. To this end, we compute the j -rank approximation of W using SVD and factor it into a pair of smaller matrices $U \in \mathbb{R}^{f \times j}$ and $V \in \mathbb{R}^{j \times c\kappa_1\kappa_2}$. More details on how to compute U and V are given in Section A. We may then replace the original convolution, represented by W , by two smaller convolutions, represented by V and U for the first and second layer, respectively. Just like for the original layer, we can establish an equivalent convolution layer for both U and V as depicted in Figure 9. To establish the equivalence we note that (a) every row of the matrices V and

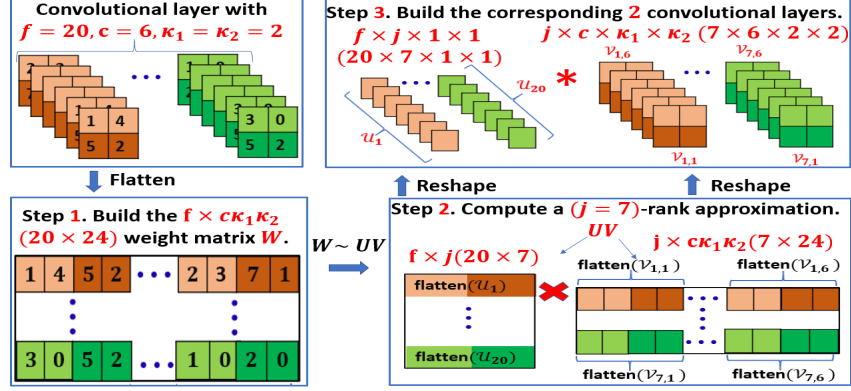


Figure 9: **Low-rank decomposition for convolutional layers via SVD.** The given convolution, c.f. Figure 8, has 20 filters, each of shape $6 \times 2 \times 2$, resulting in a total of 480 parameters. After extracting the corresponding weight matrix $W \in \mathbb{R}^{20 \times 24}$ ($f \times c\kappa_1\kappa_2$), we compute its ($j = 7$)-rank decomposition to obtain the pair of matrices $U \in \mathbb{R}^{20 \times 7}$ ($f \times j$) and $V \in \mathbb{R}^{7 \times 24}$ ($j \times c\kappa_1\kappa_2$). Those matrices are encoded back as a pair of convolutional layers, the first (corresponding to V) has $j = 7$ filters, $c = 6$ channels and a 2×2 ($\kappa_1 \times \kappa_2$) kernel, whereas the second (corresponding to U) is a 1×1 convolution of $f = 20$ filters, and $j = 7$ channels. The resulting layers have 308 parameters.

U corresponds to a flattened filter of the respective convolution, and (b) the number of channels in each layer is equal to the number of channels in its corresponding input tensor. Hence, the first layer, which is represented by $V \in \mathbb{R}^{j \times c\kappa_1\kappa_2}$ has j filters, c.f. (a), each consisting of c channels, c.f. (b), with kernel size $\kappa_1 \times \kappa_2$. The second layer corresponding to U has f filters, c.f. (a), j channels, c.f. (b), and a 1×1 kernel and may be equivalently represented as the tensor $\mathcal{U} \in \mathbb{R}^{f \times j \times 1 \times 1}$. Note that the number of weights is reduced from $f c \kappa_1 \kappa_2$ to $j(f + c \kappa_1 \kappa_2)$.

A.2 Clustering Methods

As previously explained in Section 2.1, one can cluster the columns of the corresponding weight matrix W , instead of clustering the channels of the convolutional layer. Here, the channel clustering can be defined as constraint clustering of these columns, where columns which include entries that correspond to the same kernel (e.g., the first 4 columns in W from Figure 9) are guaranteed to be in the same cluster.

This generalization is easily adaptable to other clustering methods that generate a wider set of solutions, e.g., the known ***k*-means**. An intuitive choice for our case is **projective clustering** and its variants. The goal of projective clustering is to compute a set of k subspaces, each of dimension j , that minimizes the sum of *squared* distances from each column in W to its *closest* subspace from this set. Then, we can partition the columns of W into k subsets according to their nearest subspace from this set. This is a natural extension of SVD that solves this problem for the case of $k = 1$. However, this problem is known to be NP-hard, hence expensive approximation algorithms are required to solve it, or alternatively, a local minimum solution can be obtained using the Expectation-Maximization method (EM) (Dempster et al., 1977).

A more robust version of the previous method is to minimize the sum of *non-squared* distances from the points to the subspaces. This approach is known to be more robust toward outliers (“far away points”). Similarly to the original variant (the case of squared distance), we can use the EM method to obtain a “good guess” for a solution of this problem, however, the EM method requires an algorithm that solves the problem for the case of $k = 1$, i.e., computing the subspace that minimizes the sum of (non-squared) distances from those columns (for the sum of squared distances case, SVD is this algorithm). Unfortunately, there is only approximation algorithms (Clarkson and Woodruff, 2015; Tukan et al., 2020) for this case, and the deterministic versions are expensive in terms of running time.

Furthermore, and probably more importantly, all of these methods cannot be considered as structured compression since arbitrary clustering may require re-shuffling the input tensors which could lead to significant slow-downs during inference. For example, when compressing a fully-connected layer,

the arbitrary clustering may result in nonconsecutive neurons from the first layer that are connected to the same neuron in the second layer, while neurons that are between them are not. Hence, these layers can only have a large, sparse instead of a small, dense representation.

To this end, we choose to use **channel slicing**, i.e., we simply split the channels of the convolutional layer into k chunks, where each chunk has at most c/k consecutive channels. Splitting the channels into consecutive subsets (without allowing any arbitrary clustering) and applying the factorization on each one results in a structurally compressed layer without the need of special software/hardware support. Furthermore, this approach is the fastest among all the others. Finally, while other approaches may give a better initial guess for a compressed network in theory, in practice this is not the case; see Figures 10. This is due to the global compression framework (Section 2.2) which repeatedly utilizes the channel slicing.

We see that in practice, our method improve upon state-of-the-art techniques and obtains smaller networks with higher accuracy without the use of those complicated approaches that may result in sparse but not smaller network; see Section C.3.

A.3 Compressing via SVD

As explained in Section 2.1, the weights of a convolutional layer (or a dense layer) can be encoded into a matrix $W \in \mathbb{R}^{f \times ck_1k_2}$, where f and c are the number of filters and channels in the layer, respectively, and $k_1 \times k_2$ is the size of the kernel. In order to compress the matrix W (and thus its corresponding layer) we aim to factor it into a pair of smaller matrices $U \in \mathbb{R}^{f \times j}$ and $V \in \mathbb{R}^{j \times ck_1k_2}$, such that UV approximates the original matrix operator W .

How to compute the matrices U and V ? For simplicity, let $d = ck_1k_2$. We factor the matrix $W \in \mathbb{R}^{f \times d}$ via SVD to obtain $W = \tilde{U}\tilde{\Sigma}\tilde{V}$, where \tilde{U} is an $f \times f$ orthogonal matrix, $\tilde{\Sigma}$ is an $f \times d$ rectangular diagonal matrix with non-negative real numbers on the diagonal, and \tilde{V} is an $d \times d$ orthogonal matrix.

To compute a j -rank approximation of W , we can simply define the following 3 matrices: $U \in \mathbb{R}^{f \times j}$, $\bar{V} \in \mathbb{R}^{j \times d}$, and $\Sigma \in \mathbb{R}^{j \times j}$, where U is constructed by taking the first j columns of \tilde{U} , \bar{V} by taking the first j rows of \tilde{V} , and Σ is a diagonal matrix such that the j entries on its diagonal are equal to the first j entries on the diagonal of $\tilde{\Sigma}$. Now we have that $U\Sigma\bar{V}$ is the j -rank approximation of W .

Finally, we can define $V = \Sigma\bar{V}$ to obtain a factorization of the j -rank approximation of W as UV .

A.4 Efficient Implementation of ALDS (Algorithm 1)

Our algorithm that is suggested in Section 2.2 aims at minimizing the maximum relative error $\varepsilon := \max_{\ell \in [L]} \varepsilon^\ell$ across the L layers of the network as a proxy for the true cost, where ε^ℓ is the theoretical maximum relative error in the ℓ^{th} :

$$\varepsilon^\ell := \frac{\|\hat{W}^\ell - W^\ell\|}{\|W^\ell\|}.$$

Through Algorithm 1, for every $\ell \in [L]$ we need to repeatedly compute ε^ℓ as a function of j^ℓ and k^ℓ . At Line 4, we are given a guess for the optimal values of k^1, \dots, k^L , and our goal is to compute the values j^1, \dots, j^L such that the resulting errors $\varepsilon^1, \dots, \varepsilon^L$ are (approximately) equal in order to minimize the maximum error $\max_{\ell \in [L]} \varepsilon^\ell$ while achieving the desired global compression ratio. To this end, we guess a value for ε and for given k^1, \dots, k^L pick the corresponding j^1, \dots, j^L such that ε constitutes a tight upper bound for the relative error in each layer. Based on the now resulting budget (and consequently compression ratio) we can now improve our guess of ε , e.g., via binary search or other types of root finding algorithms, until we convergence to a value of ε that corresponds to our desired overall compression ratio.

Subsequently, for each layer we are given specific values of k^ℓ and j^ℓ , which implies that we are given a budget b^ℓ for every layer $\ell \in [L]$. Subsequently, we re-assign the number of subspaces k^ℓ and their ranks j^ℓ for each layer by iterating through the finite set of possible values for k^ℓ (Line 7) and choosing the combination of j^ℓ, k^ℓ that minimizes the relative error for the current layer budget b^ℓ (computed in Line 6).

We then iteratively repeat both steps until convergence (Lines 3-8).

Hence, instead of computing the cost of each layer at each step, we can save a lookup table that stores the errors ε^ℓ for the possible values of k^ℓ and j^ℓ of each layer. For every layer $\ell \in [L]$, we iterate over the finite set of values of k^ℓ , and we split the matrix W^ℓ to k^ℓ matrices (according to the channel slicing approach that is explained in Section 2.1), then we compute the SVD factorization of each matrix from these k^ℓ matrices, and finally, compute ε^ℓ that corresponds to a specific j^ℓ (k^ℓ is already given) in $O(fd)$ time, where f is the number of rows in the weight matrix that corresponds to the ℓ th layer and d is the number of columns.

Furthermore, instead of computing each option of ε^ℓ in $O(fd)$ time, we use the derived upper bound to compute it in $O(k)$ time and saving it in the lookup table. This is done to ensure a more efficient implementation of the lookup table, and having this table ensures a more efficient implementation of Algorithm 1.

A.5 Extensions of ALDS

As mentioned in Section 2.3 ALDS can be readily extended to any desired *set* of low-rank compression techniques. Specifically, we can replace the local step of Line 7 by a search over different methods, e.g., Tucker decomposition, PCA, or other SVD compression schemes, and return the best method for a given budget. In general, we may combine ALDS with any low-rank compression as long as we can efficiently evaluate the per-layer error of the compression scheme. Note that this essentially equips us with a framework to automatically choose the per-layer decomposition technique fully automatically.

To this end, we test an extension of ALDS where in addition to searching over multiple values of k^ℓ we simultaneously search over various flattening schemes to convert a convolutional tensor to a matrix before applying SVD.

As before, let $\mathcal{W} \in \mathbb{R}^{f \times c \times \kappa_1 \times \kappa_2}$ denote the weight tensor for a convolutional layer with f filters, c input channels, and a $\kappa_1 \times \kappa_2$ kernel. Moreover, let j denote the desired rank of the decomposition. We consider the following schemes to automatically search over:

- SCHEME 0: flatten the tensor to a matrix of shape $f \times c\kappa_1\kappa_2$. The decomposed layers correspond to a $j \times c \times \kappa_1 \times \kappa_2$ -convolution followed by a $f \times j \times 1 \times 1$ -convolution. This is the same scheme as used in ALDS.
- SCHEME 1: flatten the tensor to a matrix of shape $f\kappa_1 \times c\kappa_2$. The decomposed layers correspond to a $j \times c \times 1 \times \kappa_2$ -convolution followed by a $f \times j \times \kappa_1 \times 1$ -convolution.
- SCHEME 2: flatten the tensor to a matrix of shape $f\kappa_2 \times c\kappa_1$. The decomposed layers correspond to a $j \times c \times \kappa_1 \times 1$ -convolution followed by a $f \times j \times 1 \times \kappa_2$ -convolution.
- SCHEME 3: flatten the tensor to a matrix of shape $f\kappa_1\kappa_2 \times c$. The decomposed layers correspond to a $j \times c \times 1 \times 1$ -convolution followed by a $f \times j \times \kappa_1 \times \kappa_2$ -convolution.

We denote this method by ALDS+ and provide preliminary results in Section C.4. We note that since ALDS+ is a generalization of ALDS its performance is at least as good as the original ALDS. Moreover, our preliminary results actually suggest that the extension clearly improves upon the empirical performance of ALDS.

B Experimental Setup and Hyperparameters

Our experimental evaluations are based on a variety of network architectures, data sets, and compression pipelines. In the following, we provide all necessary hyperparameters to reproduce our experiments for each of the datasets and respective network architectures.

All networks were trained, compressed, and evaluated on a compute cluster with NVIDIA Titan RTX and NVIDIA RTX 2080Ti GPUs. The experiments were conducted with PyTorch 1.7 and our code is fully open-sourced ².

²Please see supplementary material.

Table 3: The experimental hyperparameters for training, compression, and retraining for the tested **CIFAR10** network architectures. “LR” and “LR decay” hereby denote the learning and the (multiplicative) learning rate decay, respectively, that is deployed at the epochs as specified. “ $\{x, \dots\}$ ” indicates that the learning rate is decayed every x epochs.

CIFAR10	Hyperparameters		VGG16	Resnet20	DenseNet22	WRN-16-8
	(Re-)Training	Test accuracy (%)	92.81	91.4	89.90	95.19
		Loss	cross-entropy	cross-entropy	cross-entropy	cross-entropy
		Optimizer	SGD	SGD	SGD	SGD
		Epochs	300	182	300	200
		Warm-up	10	5	10	5
		Batch size	256	128	64	128
		LR	0.05	0.1	0.1	0.1
		LR decay	0.5@{30, ...}	0.1@{91, 136}	0.1@{150, 225}	0.2@{60, ...}
		Momentum	0.9	0.9	0.9	0.9
		Nesterov	✗	✗	✓	✓
		Weight decay	5.0e-4	1.0e-4	1.0e-4	5.0e-4
	Compression	α	0.80	0.80	0.80	0.80
n_{seed}		15	15	15	15	

All networks are trained according to the hyperparameters outlined in the respective original papers. During retraining, which is described in Section B.5, we reuse the same hyperparameters.

Moreover, each experiment is repeated 3 times and we report mean and mean, standard deviation in the tables and figures, respectively.

For each data set, we use the publicly available development set as test set and use a 90%/5%/5% split on the train set to obtain a separate train and *two* validation sets. One validation set is used for data-dependent compression methods, e.g., PCA (Zhang et al., 2015a); the other set is used for early stopping during training.

B.1 Experimental Setup for CIFAR10

All relevant hyperparameters are outlined in Table 3. For each of the networks we use the training hyperparameters outlined in the respective original papers, i.e., as described by He et al. (2016), Simonyan and Zisserman (2014), Huang et al. (2017), and Zagoruyko and Komodakis (2016) for ResNets, VGGs, DenseNets, and WideResNets (WRN), respectively.

We add a warmup period in the beginning where we linearly scale up the learning rate from 0 to the nominal learning rate to ensure proper training performance in distributed training settings (Goyal et al., 2017).

During training we use the standard data augmentation strategy for CIFAR: (1) zero padding from 32x32 to 36x36; (2) random crop to 32x32; (3) random horizontal flip; (4) channel-wise normalization. During inference only the normalization (4) is applied.

The compression ratios are chosen according to a geometric sequence with the common ratio denoted by α in Table 3, i.e., the compression ratio for iteration i is determined by $1 - \alpha^i$. The compression parameter n_{seed} denotes the number of seeds used to initialize Algorithm 1 for compressing with PP.

B.2 Experimental Setup for ImageNet

We report the relevant hyperparameters in Table 4. For ImageNet we consider the networks architectures Resnet18 (He et al., 2016) and AlexNet (Krizhevsky et al., 2012).

During training we use the following data augmentation: (1) randomly resize and crop to 224x224; (2) random horizontal flip; (3) channel-wise normalization. During inference, we use a center crop to 224x224 before (3) is applied.

B.3 Experimental Setup for Pascal VOC

In addition to CIFAR and ImageNet, we also consider the segmentation task from Pascal VOC 2012 Everingham et al. (2015). We augment the nominal data training data using the extra labels as

Table 4: The experimental hyperparameters for training, compression, and retraining for the tested **ImageNet** network architectures. “LR” and “LR decay” hereby denote the learning and the (multiplicative) learning rate decay, respectively, that is deployed at the epochs as specified. “ $\{x, \dots\}$ ” indicates that the learning rate is decayed every x epochs.

ImageNet	Hyperparameters		ResNet18	AlexNet
	(Re-)Training	Top 1 Test accuracy (%)	69.64	57.30
		Top 5 Test accuracy (%)	88.98	80.20
		Loss	cross-entropy	cross-entropy
		Optimizer	SGD	SGD
		Epochs	90	90
		Warm-up	5	5
		Batch size	256	256
		LR	0.1	0.1
		LR decay	$0.1@ \{30, 60, 80\}$	$0.1@ \{30, 60, 80\}$
		Momentum	0.9	0.9
		Nesterov	\times	\times
		Weight decay	$1.0e-4$	$1.0e-4$
	Compression	α	0.80	0.80
		n_{seed}	15	15

Table 5: The experimental hyperparameters for training, compression, and retraining for the tested **VOC** network architecture. “LR” and “LR decay” hereby denote the learning and the learning rate decay, respectively. Note that the learning rate is polynomially decayed after each step.

Pascal VOC 2012 – Segmentation	Hyperparameters		DeeplabV3-ResNet50
	(Re-)Training	IoU Test accuracy (%)	69.84
		Top 1 Test accuracy (%)	94.25
		Loss	cross-entropy
		Optimizer	SGD
		Epochs	45
		Warm-up	0
		Batch size	32
		LR	0.02
		LR decay	$(1 - \text{“step”}/\text{“total steps”})^{0.9}$
		Momentum	0.9
		Nesterov	\times
		Weight decay	$1.0e-4$
	Compression	α	0.80
		n_{seed}	15

provided by [Hariharan et al. \(2011\)](#). As network architecture we consider a DeeplabV3 [Chen et al. \(2017\)](#) with ResNet50 backbone pre-trained on ImageNet.

During training we use the following data augmentation pipeline: (1) randomly resize (256x256 to 1024x1024) and crop to 513x513; (2) random horizontal flip; (3) channel-wise normalization. During inference, we resize to 513x513 exactly before the normalization (3) is applied.

We report both intersection-over-union (IoU) and Top1 test accuracy for each of the compressed and uncompressed networks. The experimental hyperparameters are summarized in Table 5.

B.4 Baseline Methods

We implement and compare against the following compression methods for our baseline experiments:

1. PCA ([Zhang et al., 2015a](#)) decomposes each layer based on principle component analysis of the pre-activation (output of linear layer). We implement the symmetric, linear version of their method. The per-layer compression ratio is based on the greedy solution for minimizing the product of the per-layer energy, where the energy is defined as the sum of singular values in the compressed layer, see Equation (14) of [Zhang et al. \(2015a\)](#).

2. SVD-ENERGY (Alvarez and Salzmann, 2017; Wen et al., 2017) decomposes each layer via matrix folding akin to our SVD-based decomposition. The per-layer compression ratio is found by keeping the relative energy reduction constant across layers, where energy is defined as the sum of squared singular values.
3. SVD (Denton et al., 2014) decomposes each layer via matrix folding akin to our SVD-based decomposition. However, we hereby fix $k^\ell = 1$ for all layers $\ell \in [L]$ in order to provide a nominal comparison akin of “standard” tensor decomposition. The per-layer compression ratio is kept constant across all layers.
4. L-RANK (Idelbayev and Carreira-Perpinán, 2020) decomposes each layer via matrix folding akin to our SVD-based decomposition. The per-layer compression is determined by minimizing a joint cost objective of the energy and the computational cost of each layer, see Equation (5) of Idelbayev and Carreira-Perpinán (2020) for details.
5. FT Li et al. (2016) prunes the filters (or neurons) in each layer with the lowest element-wise ℓ_2 -norm. The per-layer compression ratio is set manually (constant in our implementation).
6. PFP Liebenwein et al. (2020) prunes the channels with the lowest sensitivity, where the data-dependent sensitivities are based on a provable notion of channel pruning. The per-layer prune ratio is determined based on the associated theoretical error guarantees.

B.5 Compress-Retrain Pipeline

Recall that our baseline experiments are based on the following unified compress-retrain pipeline across all compression methods:

1. TRAIN for e epochs according to the standard training schedule for the respective network.
2. COMPRESS the network according to the chosen method.
3. RETRAIN the network for the desired amount of r epochs using the original training hyperparameters from the epochs in the range $[e - r, e]$.
4. ITERATIVELY repeat 1.-3. after projecting the decomposed layers back (**optional**).

In addition, we also consider experiments in the iterative learning rate rewinding setting, where steps 2 and 3 are repeated iteratively (optional step 4).

While various papers combine their compression methods with different retrain schedules we unify the compress-retrain pipeline across all tested methods for our baseline experiments to ensure that results are comparable. Note that the implemented compress-retrain pipeline as originally introduced by Renda et al. (2020) has been shown to yield consistently good compression results across various compression/pruning setups (unstructured, structured) and tasks (computer vision, NLP). Hence, we choose to concentrate on that particular pipeline.

C Additional Experimental Results

In this section, we provide additional results of our experimental evaluations.

C.1 Complete Tables for One-shot Compression Experiments from Section 3.1

Table 6: The maximal compression ratio for which the drop in test accuracy is at most some pre-specified δ on CIFAR10. The table reports compression ratio in terms of parameters and FLOPs, denoted by CR-P and CR-F, respectively. When the desired δ was not achieved for any compression ratio in the range the fields are left blank. The top values achieved for CR-P and CR-F are bolded.

Model	Prune Method	$\delta = 0.0\%$			$\delta = 0.5\%$			$\delta = 1.0\%$			$\delta = 2.0\%$			$\delta = 3.0\%$			
		Top1 Acc.	CR-P	CR-F	Top1 Acc.	CR-P	CR-F	Top1 Acc.	CR-P	CR-F	Top1 Acc.	CR-P	CR-F	Top1 Acc.	CR-P	CR-F	
CIFAR10	ResNet20 Top1: 91.39	ALDS	+0.09	64.58	55.95	-0.47	74.91	67.86	-0.68	79.01	71.59	-1.88	87.68	83.23	-2.59	89.65	85.32
		PCA	+0.16	39.98	38.64	-0.11	49.88	48.67	-0.58	58.04	57.21	-1.41	70.54	70.78	-2.11	75.23	76.01
		SVD-Energy	+0.14	40.22	39.38	-0.21	49.88	49.08	-0.83	57.95	57.15	-1.52	64.76	64.10	-2.17	70.47	70.01
		SVD	+0.24	14.36	15.34	-0.29	39.81	38.95	-0.90	49.19	50.21	-1.08	57.47	57.80	-2.88	70.14	71.31
		L-Rank	+0.14	15.00	29.08	-0.44	28.71	54.89	-0.44	28.71	54.89	-1.56	49.87	72.57	-2.82	64.81	80.80
		FT	+0.15	15.29	16.66	-0.32	39.69	39.57	-0.75	57.77	55.85	-1.88	74.89	71.76	-2.71	79.29	76.74
		PFP	+0.12	28.74	20.56	-0.28	40.28	30.06	-0.85	58.26	46.94	-1.56	70.49	59.78	-2.57	79.28	69.27
	VGG16 Top1: 92.78	ALDS	+0.29	94.89	83.94	-0.11	95.77	86.23	-0.52	97.01	88.95	-0.52	97.03	88.95	-0.52	97.03	88.95
		PCA	+0.47	87.74	81.05	-0.02	89.72	85.84	-0.02	89.72	85.84	-1.12	91.37	89.57	-1.12	91.37	89.57
		SVD-Energy	+0.35	79.21	78.70	-0.08	82.57	81.32	-0.83	87.74	85.36	-1.22	89.71	87.13	-2.08	91.37	88.58
		SVD	+0.29	70.35	70.13	+0.29	70.35	70.13	-0.74	75.18	75.13	-1.58	82.58	82.39	-1.58	82.58	82.39
		L-Rank	+0.35	82.56	69.67	-0.35	85.38	75.86	-0.35	85.38	75.86	-0.35	85.38	75.86	-0.35	85.38	75.86
		FT	+0.17	64.81	62.16	-0.47	79.13	78.44	-0.87	82.61	82.41	-1.95	89.69	89.91	-2.66	91.35	91.68
		PFP	+0.16	89.73	74.61	-0.47	94.87	84.76	-0.96	96.40	88.38	-1.33	97.02	90.25	-1.33	97.02	90.25
	DenseNet22 Top1: 89.88	ALDS	+0.17	48.85	51.90	-0.32	56.84	61.98	-0.54	63.83	69.68	-1.87	69.67	74.48	-1.87	69.67	74.48
		PCA	+0.20	14.67	34.55	+0.20	14.67	34.55	-0.73	28.83	57.02	-0.73	28.83	57.02	-2.75	40.51	70.03
		SVD-Energy				-0.29	15.16	19.34	-0.29	15.16	19.34	-1.28	28.62	33.26	-2.21	40.20	44.72
		SVD	+0.13	15.00	15.33	+0.13	15.00	15.33	-0.87	26.73	27.41	-0.87	26.73	27.41	-2.51	37.99	39.25
		L-Rank	+0.26	14.98	35.21	+0.26	14.98	35.21	-0.90	28.67	63.55	-1.82	40.33	73.45	-1.82	40.33	73.45
		FT	+0.15	15.49	16.70	-0.24	28.33	29.50	-0.24	28.33	29.50	-1.46	51.10	51.03	-2.40	64.12	63.09
		PFP	+0.00	28.68	32.60	-0.44	40.24	43.37	-0.70	49.67	51.94	-1.36	58.20	58.21	-2.43	65.17	64.50
	WRN16-8 Top1: 95.21	ALDS	+0.05	28.67	13.00	-0.42	87.77	79.90	-0.88	92.75	87.39	-1.53	95.09	92.50	-2.23	97.01	95.51
		PCA	+0.14	15.00	7.98	-0.49	85.33	83.45	-0.96	91.33	90.23	-1.76	93.90	93.15	-2.45	94.87	94.30
		SVD-Energy	+0.29	15.01	6.92	-0.41	64.75	60.94	-0.81	85.38	83.52	-1.90	91.38	90.04	-2.46	92.77	91.58
		SVD				-0.96	40.20	39.97	-1.63	70.48	70.49	-1.63	70.48	70.49	-1.63	70.48	70.49
		L-Rank	+0.25	14.99	6.79	-0.45	49.86	58.00	-0.88	75.20	82.26	-1.70	87.73	92.03	-2.18	89.72	93.51
		FT	+0.03	64.54	61.53	-0.32	82.33	75.97	-0.95	89.70	83.52	-1.78	94.91	90.82	-2.86	96.42	93.33
		PFP	+0.05	57.92	54.74	-0.44	85.33	80.68	-0.77	89.71	85.16	-1.69	95.65	92.60	-2.40	96.96	94.36

Table 7: The maximal compression ratio for which the drop in test accuracy is at most $\delta = 1.0\%$ for ResNet20 (CIFAR10) for various amounts of retraining (as indicated). The table reports compression ratio in terms of parameters and FLOPs, denoted by CR-P and CR-F, respectively. When the desired δ was not achieved for any compression ratio in the range the fields are left blank. The top values achieved for CR-P and CR-F are bolded.

Model	Prune Method	$r = 0\%$ e			$r = 5\%$ e			$r = 10\%$ e			$r = 25\%$ e			$r = 50\%$ e			$r = 100\%$ e			
		Top1 Acc.	CR-P	CR-F	Top1 Acc.	CR-P	CR-F	Top1 Acc.	CR-P	CR-F	Top1 Acc.	CR-P	CR-F	Top1 Acc.	CR-P	CR-F	Top1 Acc.	CR-P	CR-F	
CIFAR10	ResNet20 Top1: 91.39	ALDS	-0.13	14.82	7.03	-0.53	35.87	26.27	-0.73	43.12	33.65	-0.65	43.14	33.33	-0.86	62.39	54.40	-0.88	81.29	74.23
		PCA							-0.74	19.31	18.64	-0.70	19.34	18.44	-0.59	36.21	35.19	-0.74	60.29	59.81
		SVD-Energy				-0.64	14.99	14.09	-0.70	19.61	18.81	-0.59	19.61	18.81	-0.73	43.46	42.49	-0.46	55.25	54.59
		SVD							-0.58	14.36	15.34	-0.64	15.00	29.08	-0.33	15.00	29.08	-0.44	28.71	54.89
		L-Rank							-0.67	15.29	16.66	-0.69	27.76	28.40	-0.69	27.76	28.40	-0.75	57.77	55.85
		FT							-0.77	14.88	9.61	-0.83	32.71	23.85	-0.83	32.71	23.85	-0.54	52.89	42.04
		PFP																		

Table 8: The maximal compression ratio for which the drop in test accuracy is at most some pre-specified δ on ResNet18 (ImageNet). The table reports compression ratio in terms of parameters and FLOPs, denoted by CR-P and CR-F, respectively. When the desired δ was not achieved for any compression ratio in the range the fields are left blank. The top values achieved for CR-P and CR-F are bolded.

Model	Prune Method	$\delta = 0.0\%$			$\delta = 0.5\%$			$\delta = 1.0\%$			$\delta = 2.0\%$			$\delta = 3.0\%$			
		Top1/5 Acc.	CR-P	CR-F	Top1/5 Acc.	CR-P	CR-F	Top1/5 Acc.	CR-P	CR-F	Top1/5 Acc.	CR-P	CR-F	Top1/5 Acc.	CR-P	CR-F	
ImageNet	ResNet18 Top1: 69.64 Top5: 88.98	ALDS	+0.24/+0.39	50.33	23.62	-0.40/-0.05	66.70	43.51	-0.40/-0.05	66.70	43.51	-1.58/-0.55	77.62	59.51	-2.70/-1.39	81.69	66.68
		PCA							-0.95/-0.37	9.99	12.78	-1.71/-0.85	50.42	51.68	-2.40/-1.06	59.38	60.04
		SVD-Energy							-1.49/-0.64	39.56	40.99	-1.75/-0.72	50.38	50.37	-2.90/-1.38	59.43	60.65
		SVD							-0.71/-0.23	10.01	32.64	-0.71/-0.23	10.01	32.64	-2.38/-1.38	26.24	59.82
		L-Rank							-0.66/-0.17	26.08	26.44	-1.83/-0.73	39.88	38.13	-2.99/-1.41	50.33	47.18
		FT	+0.10/+0.42	9.86	11.17	+0.10/+0.42	9.86	11.17	-0.39/-0.08	26.35	17.96	-1.62/-0.71	39.66	27.71	-1.62/-0.71	39.66	27.71
		PFP	+0.36/+0.51	10.09	7.35	-0.39/-0.08	26.35	17.96									

Table 9: The maximal compression ratio for which the drop in test accuracy is at most $\delta = 1.0\%$ for ResNet18 (ImageNet) for various amounts of retraining (as indicated). The table reports compression ratio in terms of parameters and FLOPs, denoted by CR-P and CR-F, respectively. When the desired δ was not achieved for any compression ratio in the range the fields are left blank. The top values achieved for CR-P and CR-F are bolded.

	Model	Prune Method	$r = 0\% e$			$r = 5\% e$			$r = 10\% e$			$r = 25\% e$			$r = 50\% e$			$r = 100\% e$		
			Top1/5 Acc.	CR-P	CR-F	Top1/5 Acc.	CR-P	CR-F	Top1/5 Acc.	CR-P	CR-F	Top1/5 Acc.	CR-P	CR-F	Top1/5 Acc.	CR-P	CR-F	Top1/5 Acc.	CR-P	CR-F
			-0.54/-0.24	39.57	15.20	-0.48/-0.24	50.46	23.70	-0.72/-0.30	53.50	26.90	-0.64/-0.31	61.90	36.58	-0.40/-0.23	68.78	47.23	-0.73/-0.31	70.73	49.85
ImageNet	ResNet18 Top1: 69.62 Top5: 89.08	ALDS							-inf/-inf	3.33	3.99	-0.80/-0.38	26.21	27.53	-0.76/-0.51	39.53	40.45	-inf/-inf	6.65	8.14
		PCA							-0.25/-0.12	10.00	11.05	-0.55/-0.25	26.24	27.14	-0.66/-0.33	39.56	40.48	-inf/-inf	3.33	3.66
		SVD-Energy				-0.28/-0.14	10.00	11.05	-0.19/-0.07	9.98	9.94	-0.71/-0.34	30.63	30.82	-0.59/-0.32	39.53	39.51	-inf/-inf	3.33	3.31
		SVD				-0.32/-0.13	9.98	9.94	-inf/-inf	3.34	10.88	-0.40/-0.23	10.01	32.40	-0.16/+0.03	10.01	32.40	-0.72/-0.26	10.01	32.40
		L-Rank							-inf/-inf	3.36	3.75	-0.21/-0.15	9.95	10.78	-0.83/-0.46	26.29	26.57	-0.66/-0.32	26.12	26.62
		FT							-inf/-inf	3.34	2.37	-0.14/-0.13	9.96	7.72	-0.37/-0.31	20.76	15.14	-0.38/-0.15	26.35	19.14
		PEP																		

Table 10: The maximal compression ratio for which the drop in test accuracy is at most some pre-specified δ on DeeplabV3-ResNet50 (Pascal VOC2012). The table reports compression ratio in terms of parameters and FLOPs, denoted by CR-P and CR-F, respectively. When the desired δ was not achieved for any compression ratio in the range the fields are left blank. The top values achieved for CR-P and CR-F are bolded.

	Model	Prune Method	$\delta = 0.0\%$			$\delta = 0.5\%$			$\delta = 1.0\%$			$\delta = 2.0\%$			$\delta = 3.0\%$		
			IoU/Top1 Acc.	CR-P	CR-F	IoU/Top1 Acc.	CR-P	CR-F	IoU/Top1 Acc.	CR-P	CR-F	IoU/Top1 Acc.	CR-P	CR-F	IoU/Top1 Acc.	CR-P	CR-F
			+0.14/-0.15	64.38	64.11	+0.14/-0.15	64.38	64.11	+0.14/-0.15	64.38	64.11	-1.22/-0.36	71.36	70.89	-2.76/-0.61	76.96	76.37
VOC Segmentation2012	DeeplabV3-ResNet50 IoU: 68.16 Top1: 94.25	ALDS				-0.26/-0.02	31.59	31.63	-0.88/-0.24	55.68	55.82	-1.74/-0.39	64.33	64.54	-2.54/-0.46	71.29	71.63
		PCA										-1.88/-0.47	31.61	32.27	-2.78/-0.62	44.99	45.60
		SVD-Energy	+0.01/-0.02	14.99	14.85	-0.28/-0.18	31.64	31.51	-0.89/-0.25	45.02	44.95	-1.97/-0.50	64.42	64.42	-1.97/-0.50	64.42	64.42
		SVD				-0.42/-0.09	44.99	45.02	-0.42/-0.09	44.99	45.02	-1.29/-0.33	55.74	56.01	-2.50/-0.57	64.39	64.82
		L-Rank															
		FT															
		PEP	+0.01/-0.05	31.79	30.62	-0.49/-0.21	45.17	43.93	-0.84/-0.32	55.78	54.61	-0.84/-0.32	55.78	54.61	-2.43/-0.61	64.47	63.41

C.2 Complete ImageNet Benchmark Results from Section 3.2

Results are provided in Table 11.

C.3 Ablation Study

In order to gain a better understanding of the various aspects of our method we consider an ablation study where we selectively turn off various features of ALDS. Specifically, we compare the full version of ALDS to the following variants:

1. ALDS-ERROR solves for the optimal ranks (Line 4 of Algorithm 1) for a desired set of values for k^1, \dots, k^L . We test $k^\ell = 3, \forall \ell \in [L]$. This variant tests the benefits of varying the number of subspaces compared to fixing them to a desired value.
2. SVD-ERROR corresponds to ALDS-Error with $k^\ell = 1, \forall \ell \in [L]$. This variant tests the benefits of having multiple subspaces in the first places in the context error-based allocation of the per-layer compression ratio.
3. ALDS-SIMPLE picks the ranks in each layer for a desired set of values of k^1, \dots, k^L such that the per-layer compression ratio is constant. We test $k^\ell = 3, \forall \ell \in [L]$, and $k^\ell = 5, \forall \ell \in [L]$. This variant tests the benefits of allocating the per-layer compression ratio according to the layer error compared to a simple constant heuristic.
4. MESSI proceeds like ALDS-Simple but replaces the subspace clustering with projective clustering (Maalouf et al., 2021). We test $k^\ell = 3, \forall \ell \in [L]$. This variant tests the disadvantages of having a simple subspace clustering technique (channel slicing) compared to using a more sophisticated technique.

We note that ALDS-Simple with $k^\ell = 1, \forall \ell \in [L]$ corresponds to the SVD comparison method from the previous sections.

We study the variations on a ResNet20 trained on CIFAR10 in two settings: compression only and one-shot compress+retrain. The results are presented in Figures 10. We highlight that the complete variant of our algorithm (ALDS) consistently outperforms the weaker variants providing empirical evidence on the effectiveness of each of the core components of ALDS.

We note that varying the number of subspaces for each layer in order to optimally assign a value of k^ℓ in each layer is crucial in improving our performance. This is apparent from the comparison between ALDS, ALDS-Error, and SVD-Error: having a fixed value for k yields sub-optimal results.

Picking an appropriate notion of cost (maximum relative error) is furthermore preferred over simple heuristics such as a constant per-layer compression ratio. Specifically, the main difference between ALDS-Error and ALDS-Simple is the way how the ranks are determined for a given set of k 's: ALDS-Error optimizes for the error-based cost function while ALDS-Simple relies on a simple constant per-layer compression ratio heuristic. In practice, ALDS-Error outperforms ALDS-Simple across all tested scenarios.

Finally, we test the disadvantages of using a simple subspace clustering method. To this end, we compare ALDS-Simple and Messi for fixed values of k . While in some scenarios, particularly without retraining, Messi provides modest improvements over ALDS-Simple, the improvement is negligible for most settings. Moreover, note that Messi requires an expensive approximation algorithm as explained in Section A.2. This would in turn prevent us from incorporating Messi into the full ALDS framework in a computationally efficient manner. However, as apparent from the ablation study we exhibit the most performance gains for features related to global considerations instead of local, per-layer improvements. In addition, we should also note that Messi does not emit a structured reparameterization thus requires specialized software or hardware to obtain speed-ups. Consequently, we may conclude that channel slicing is the appropriate clustering technique in our context.

Table 11: AlexNet and ResNet18 Benchmarks on ImageNet. We report Top-1, Top-5 accuracy and percentage reduction in terms of parameters and FLOPs denoted by CR-P and CR-F, respectively. Best results with less than 0.5% accuracy drop are **bolded**.

	Method	Δ -Top1	Δ -Top5	CR-P (%)	CR-F (%)
ResNet18, Top1, 5: 69.64%, 88.98%	ALDS (Ours)	+0.41	+0.37	66.70	42.70
	ALDS (Ours)	-0.38	+0.04	75.00	64.50
	ALDS (Ours)	-0.90	-0.25	78.50	71.50
	ALDS (Ours)	-1.37	-0.56	80.60	76.30
	MUSCO (Gusak et al., 2019)	-0.37	-0.20	N/A	58.67
	TRP1 (Xu et al., 2020)	-4.18	-2.5	N/A	44.70
	TRP1+Nu (Xu et al., 2020)	-4.25	-2.61	N/A	55.15
	TRP2+Nu (Xu et al., 2020)	-4.3	-2.37	N/A	68.55
	PCA (Zhang et al., 2015b)	-6.54	-4.54	N/A	29.07
	Expand (Jaderberg et al., 2014)	-6.84	-5.26	N/A	50.00
	PFP (Liebenwein et al., 2020)	-2.26	-1.07	43.80	29.30
	SoftNet (He et al., 2018)	-2.54	-1.2	N/A	41.80
	Median (He et al., 2019)	-1.23	-0.5	N/A	41.80
	Slimming (Liu et al., 2017)	-1.77	-1.19	N/A	28.05
	Low-cost (Dong et al., 2017)	-3.55	-2.2	N/A	34.64
	Gating (Hua et al., 2018)	-1.52	-0.93	N/A	37.88
	FT (He et al., 2017)	-3.08	-1.75	N/A	41.86
	DCP (Zhuang et al., 2018)	-2.19	-1.28	N/A	47.08
	FBS (Gao et al., 2018)	-2.44	-1.36	N/A	49.49
AlexNet, Top1, 5: 57.30%, 80.20%	ALDS (Ours)	+0.10	+0.45	92.00	76.10
	ALDS (Ours)	-0.21	-0.36	93.0	77.9
	ALDS (Ours)	-0.41	-0.54	93.50	81.4
	Tucker (Kim et al., 2015a)	N/A	-1.87	N/A	62.40
	Regularize (Tai et al., 2015)	N/A	-0.54	N/A	74.35
	Coordinate (Wen et al., 2017)	N/A	-0.34	N/A	62.82
	Efficient (Kim et al., 2019)	-0.7	-0.3	N/A	62.40
	L-Rank (Idelbayev et al., 2020)	-0.13	-0.13	N/A	66.77
	NISP (Yu et al., 2018)	-1.43	N/A	N/A	67.94
	OICSR (Li et al., 2019a)	-0.47	N/A	N/A	53.70
	Oracle (Ding et al., 2019)	-1.13	-0.67	N/A	31.97

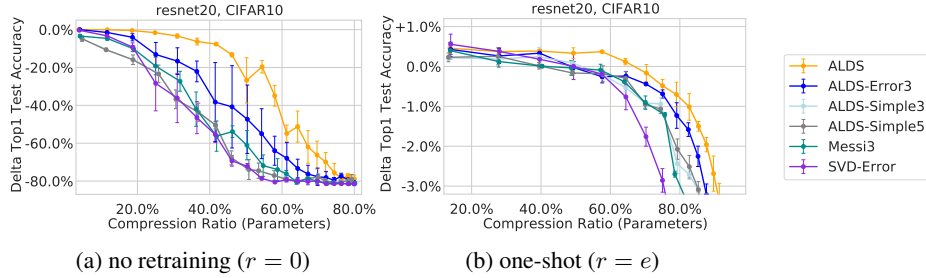


Figure 10: The difference in test accuracy (“Delta Top1 Test Accuracy”) for various target compression ratios, ALDS-based/ALDS-related methods, and networks on CIFAR10.

C.4 Extensions of ALDS

We test and compare ALDS with ALDS+ (see Section A.5) to investigate the performance gains we can obtain from generalizing our local step to search over multiple decomposition schemes. We run one-shot compress-only experiments on ResNet20 (CIFAR10) and ResNet18 (ImageNet).

The results are shown in Figure 11. We find that ALDS+ can significantly increase the performance-size trade-off compared to our standard ALDS method. This is expected since by generalizing the local step of ALDS we are increasing the search space of possible decomposition solution. Using our ALDS framework we can efficiently and automatically search over the increases solution space. We envision that our observations will invigorate future research into the possibility of not only choosing the optimal per-layer compression ratio but also the optimal compression scheme.

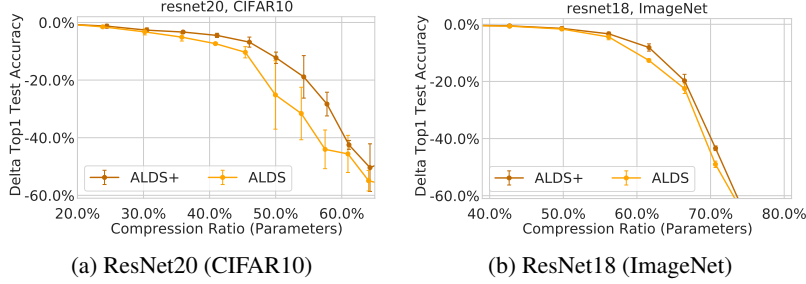


Figure 11: The difference in test accuracy (“Delta Top1 Test Accuracy”) for various target compression ratios, ALDS-based/ALDS-related methods, and networks on CIFAR10. The networks were compressed once and not retrained afterwards.